SYN- AND POST-ERUPTIVE CONTROLS ON CINDER CONE MORPHOLOGY AND DISTRIBUTION IN THE NYAMBENI HILLS VOLCANIC FIELD, KENYA

By

MARGOT MELISA FERENCZ

Graduate School-New Brunswick

Rutgers, The State University of New Jersey

In partial fulfillment of the requirements

For the degree of

Master of Science

Graduate Program in Geological Science

Written under the direction of

Karen G. Bemis

And approved by

_____

_____

_____

_____

New Brunswick, New Jersey

May, 2015

ABSTRACT OF THE THESIS

SYN- AND POST-ERUPTIVE CONTROLS ON CINDER CONE MORPHOLOGY AND DISTRUBTION IN THE NYAMBENI HILLS VOLCANIC FIELD, KENYA

by MARGOT MELISA FERENCZ

Thesis Director:

Karen G. Bemis

Syn- and post-eruptive controls on cinder cone morphology are identified in the Nyambeni Hills volcanic field of Kenya. The morphology of 65 cinder cones in the Nyambeni Hills volcanic field including cone height, crater width, and basal width in addition to the ellipticity and azimuth of elongation of 372 craters were measured using a combination of topographical maps, publically available satellite imagery, and freely downloadable digital elevation models (DEM). Morphological data from the Nyambeni Hills volcanic field are compared with the morphology of cones from two subduction-associated cinder cone fields (the Guatemalan Salvadorian volcanic field of Central America and the Lamongan volcanic field of Indonesia) and one rift-associate field (the Cima volcanic field of California) to better understand the role of tectonic setting and climate on cone morphology. In the Nyambeni Hills volcanic field the tectonic regime is the most influential factor on cone morphology and distribution. Cone morphologies both corroborate and refute outstanding predictions about subduction-associated cones versus intraplate rift-

associated cones. Cones within the Nyambeni Hills volcanic field are more elongated than those from the Guatemalan Salvadorian volcanic field and have an average axial ratio of 0.74. Elongated cones from the Nyambeni Hills display a preferential NNE orientation compatible with an east-west regional extension model over the lifetime of the volcanic field. The orientation of the entire field trends more NE than the signal preserved by elongated cones. Morphological trends in the Nyambeni Hills volcanic field support the hypothesis that the youngest cinder cones are located in the center of the field and are progressively older moving east or west. Differences in cone distribution between the north and south ends of the Nyambeni Hills in addition to age-related morphological trends attest to magma supply heterogeneity and the centralization of the magmatic system over time. Cinder cone morphology from the four study sites shows either no correlation or very weak correlations between morphological parameters and climate.

ACKNOWLEDGEMENTS

First I'd like to extend a very warm thank you to my academic advisor Dr. Karen G. Bemis for her critical support, mentorship, and guidance. Thank you to my committee members, Dr. Gail Ashley and Dr. Brent Turrin for your helpful comments and suggestions. This research would not have been possible without the financial support of Rutgers New Brunswick Graduate School and the Rutgers University Department of Earth and Planetary Sciences.

I'd like to thank Dr. Martha Withjack and Dr. Roy Schlische for enabling me to understand the structural implications of my research. The mentorship of graduate students was invaluable to me throughout my research. I'd like in particular to thank Sara Mana for her help in the lab during my first years of school. Thank you to the Earth and Planetary Sciences staff, especially Jovani Reaves, for providing so much help with the non-research parts of graduate school.

Thank you to my wonderful partner Niki for providing me with much needed technical support and for helping me continue when I felt overwhelmed. A big thank you to my family, especially my mom, dad, sister, and Uncle Juan for their unwavering support and for always providing a much needed shoulder to cry on. Finally, thank you to the local climbing community and to my friends, especially Maria Qadri and Kendra McKoy, for the laughs and for reminding me of all the good things outside of school.

TABLE OF CONTENT

Page

LIST OF FIGURES

LIST OF TABLES

INTRODUCTION

Cinder cones are the most common subaerial volcanic landform. Conical in shape, they build up by the accumulation of pyroclastic fragments during Hawaiian, Strombolian, violent Strombolian, or phreatomagmatic eruptions of basaltic magma (Martin and Németh, 2006; McGetchin et al., 1974; Valentine and Gregg, 2008). The term 'monogenetic' is widely used in reference to cinder cones because they typically form from a single eruptive episode lasting hours to months (Wood, 1980a). Cinder cones can either erupt from a central vent or as a few localized points along a fissure (Corazzato and Tibaldi, 2006; Riedel et al., 2003). Scoria cones often erupt in clusters, either as an isolated volcanic field (Hasenaka and Carmichael, 1985a; Inbar and Risso, 2001) or as parasitic cones on the flanks of a polygenetic volcano (Corazzato and Tibaldi, 2006; Kervyn et al., 2012).

The morphology and distribution of cinder cones result from both syn- and post-eruptive factors. Syn-eruptive controls include tectonic setting (Fornaciai et al., 2012; Le Corvec et al., 2013b), wind conditions (Kervyn et al., 2012), basal slope (Tibaldi, 1995), style of eruption (Valentine and Gregg, 2008), magma conduit geometry (Kervyn et al., 2012; Corazzato and Tibaldi, 2006) and crustal thickness (Mazzarini, 2004). Post-eruptive factors are degradational, and include age, weathering, erosion, and burial or modification by subsequent eruptions (Favalli et al., 2009; Hooper and Sheridan, 1998; Wood, 1980b).

Early population studies of cinder cones established the theory of an 'ideal' cone that degrades progressively with time via characteristic morphological changes (Dohrenwend et al., 1986; Hasenaka and Carmichael, 1985a; Porter, 1972;

Wood, 1980b). Recent studies highlight the complexity of syn- and post-eruptive controls on geomorphology, undermining the idea that pristine cinder cones display 'ideal' morphometric ratios and questioning the accuracy of morphology based age schemes and inferences about tectonic or eruptive conditions (Bemis et al., 2011; Kereszturi et al., 2013; Kervyn et al., 2012).

Despite the complexities of syn- and post-eruptive controls, the morphology and distribution of cinder cones can provide insights into the underlying magmatic system. The goal of this study is to identify syn- and post-eruptive morphological controls on a population of cinder cones in the Nyambeni Hills, Kenya. Once these factors are identified, cone morphology and distribution will contribute to the understanding of the magmatic system and governing tectonic regime.

The Nyambeni Hills volcanic field provides a unique opportunity to examine the controls on cinder cone morphology. It is a suitable candidate for this study because it experiences internal climate diversity. This will allow me to systematically study the effects of climate on cinder cone morphology. To broaden the climate range represented in this study and to understand the Nyambeni Hills data in a global context, I have included published geomorphological data from the Guatemala Salvadorian volcanic field, Cima volcanic field, and Lamongan volcanic field.

Few studies have focused on the Nyambeni Hills volcanic field and little is known about the underlying magmatic system and how it relates to the nearby East African Rift (Aurisicchio et al., 1983; Bosworth, 1987; Brotzu et al., 1983; 1984; Hackman et al., 1990). Information gleaned about the ascendant tectonics and

magmatic system from the analysis of cinder cone morphology and distribution will provide much need data for this poorly understood section of the East African Rift System.

BACKGROUND

The ideal cone parameters proposed by Porter (1972), Settle (1979), and Wood (1980b) were suggested as average values for young cinder cones, unmodified by post-emplacement degradation. Ideal parameters were based on averages from large population studies of parasitic cones and volcanic fields across a variety of climates and tectonic settings. All three studies concluded that a height-to-basal width (Hco/Wco) ratio of 0.18, a crater width-to-basal width (Wcr/Wco) ratio of 0.40, and a slope of about 33° could reasonably describe pristine cinder cones regardless of size or lava chemistry. Settle (1979) acknowledged a wide scatter in morphological data and postulated that an Hco/Wco value of 0.20 might better represent fresh cinder cones. Numerical studies and analogue models have reproduced ideal ratios while simultaneously highlighting how variations in eruption dynamics and regional setting can produce fresh cones with non-ideal morphometries (Bemis et al., 2011; Kervyn et al., 2012; Riedel et al., 2003).

Controls on cinder cone morphology

Tectonic regime and magma supply

The tectonic regime can affect both cinder cone morphology and distribution (Fornaciai et al., 2012; Le Corvec et al., 2013b; Tibaldi, 1995). The tectonic regime's primary influence on cinder cones results from the interdependent relationship between the tectonic stress field and dike formation. Cinder cone magmas propagate to the surface via dikes whose geometry through the brittle crust is governed by a combination of two competing influences (1) the formation of new fractures perpendicular to the least compressive stress σ3, and (2) the reactivation of pre-existing fractures parallel to sub-parallel the maximum principle stress, σ1 (Delaney et al., 1986; Jolly and Sanderson, 1997; Le Corvec et al., 2013a; Rubin, 1995; Ziv et al., 2000). As shown in Figure 1, the tectonic regime determines the orientation of the principle compressive stresses within the tectonic stress field. In a purely extensional tectonic setting σ1 is vertical. In a strike-slip environment σ1 is horizontal. In both settings σ3 is perpendicular to σ1. As a consequence of differences in σ1 and σ3 orientation, newly formed dikes will have distinctive orientations in strike-slip and extensional environments.

Magma pressure also exerts some control on dike orientation (Jolly and Sanderson, 1997; Rubin, 1995). Highly buoyant magma can re-open pre-existing fractures oblique to the maximum compressive stress, σ1 (Jolly and Sanderson, 1997; Ziv et al., 2000). In areas where the magma pressure is high, feeder dikes will

exhibit multiple orientations both parallel and oblique to the maximum compressive stress (Jolly and Sanderson, 1997; Le Corvec et al., 2013b)

Population studies by Tibaldi (1995), Corazzato and Tibaldi (2006), and Le Corvec et al. (2013b) and laboratory experiments by Kervyn et al. (2012) highlight the relationship between the geometry of feeder dikes and cinder cone distribution and morphology. At the surface, feeder dikes transform into magma conduits that manifest along a spectrum between two end members (Figure 2) (Corazzato and Tibaldi, 2006). The first end member (type 1) is expressed as a single cone, circular or slightly elongated, that forms when a feeder dike is constrained by high tectonic stress or low magma pressure. The other end member (type 5), forms when a feeder dike is constrained by low tectonic stress or high magma pressure. This end member is represented as fissures or strongly elongated, relatively large cones, formed along multiple eruption points. Intermediate cones (types 2-4) can have overlapping craters or two distinct crater openings. Cinder cones formed in normal extensional environments are more elongated and display characteristics of higher types than those erupted in transtensional environments (Tibaldi, 1995). Cone elongation is manifest in both the cone base and the crater. In morphometric studies, crater ellipticity is the preferred proxy for cone elongation because the base of a cinder cone is easily modified by subsequent eruptions or erosion (Paulsen and Wilson, 2010; Tibaldi, 1995). For cones built on a background slope of < 12°, the azimuth of elongation, represented as the long axis of an elliptical cone base or crater, will be parallel to the underlying feeder dike (Kervyn et al., 2012; Paulsen and Wilson, 2010; Tibaldi, 1995). When cones related to a single magma feeding

fracture form a volcanic lineament, the azimuths of elongation will be parallel to the vent alignment because both reflect the feeder dike orientation (Figure 3).

Sand models by Kervyn et al. (2012) demonstrate how changes in the height and diameter of the magma conduit affect cone morphology. They observe that increasing the diameter of the magma conduit or raising the vent height within a cinder cone lowers the Hco/Wco and increases the Wcr/Wco ratios. Previous studies (Riedel et al., 2003; Porter, 1972) assumed that the vent is always located at the cone base and did not account for magma conduit heterogeneity when justifying scatter in cinder cone morphology.

The population-wide spatial distribution of vents within a volcanic field is thought to represent the shape of the underlying magma supply (Condit and Connor, 1996; Le Corvec et al., 2013b; Spörli and Eastwood, 1997). For example, the Auckland volcanic field of New Zealand has a sharp ellipsoid boundary hypothesized by Spörli et al. (1997) to reflect a lens shaped magma source. The Springerville volcanic field of Arizona is characterized by petrologically diverse, high vent-density clusters. Condit and Conner (1996) postulate that the clusters reflect localized, short-lived pockets of magma. Le Corvec et al. (2013b)'s study of cinder cone distribution within 37 volcanic fields found that in 75% of study sites, the orientation of the entire cone population was different than the orientation of individual volcanic lineaments. They attribute this mismatch to the sub-vertical path dikes take through the crust.

Eruption dynamics

Eruption dynamics have a strong impact on cinder cone morphology. Considering that cinder cones form via the accumulation of pyroclastic fragments, ejecta characteristics such as size, distribution, and temperature determine not only the morphology of fresh cones, but also how they will weather over time. Ejecta characteristics are determined by eruption style. Internally driven cinder cone eruptions are limited to three types defined by mass flux and clast size: Hawaiian (least explosive), Strombolian (intermediate), and violent Strombolian (most explosive) (Valentine and Gregg, 2008). Analogue models by Riedel et al. (2003) show that increasing the proportion of fine cohesive material in cinder cones results in steeper slopes and smaller craters (Figure 4A). The implication of these models is that cones formed by very explosive eruptions, where fragmentation is high, will have steeper slopes and smaller craters than cones formed by less explosive eruptions. This hypothesis is supported by Fornaciai et al. (2012)'s findings that cinder cones associated with subduction arcs, considered relatively volatile rich because of water contributed from slab dehydration, are steeper, larger, and have lower Wcr/Wco values than intraplate cones (Figure 4B).

Eruption styles are time dependent and may change throughout an eruption (Bemis et al., 2011; Kereszturi and Németh, 2012; Valentine and Gregg, 2008). Wood (1980a) for example, noted that some cones experience volatile depletion at the end of an eruptive cycle, causing the clast size to increase. Large particles more efficiently retain heat, welding slope deposits and ultimately resulting in steeper cones. Slope welding affects not only the morphology of newly formed cones but

also the erosion patterns of aging cones (Hooper and Sheridan, 1998). Welded cone rims are more resistant to erosion and welded slopes prevent the formation of gullies (Hooper and Sheridan, 1998). Bemis et al. (2011) also acknowledges the time-dependent nature of eruptions by attributing some of the morphometric variability within cinder cone populations to the presence of immature cones that cease erupting before they could reach the angle of repose.

Climate

Post-eruptive diversity is responsible for some of the scatter in cinder cone morphological data (Kereszturi and Németh, 2012; Wood, 1980b). Degradational cinder cone modification is limited to three types: burial or modification of the flanks by subsequent eruptions, mass wasting, and erosion (Wood, 1980b). By carefully identifying the basal slope, researchers can account for flank burial and eliminate its effects on morphological measurements of cone height and basal width (Favalli et al., 2009). Mass wasting of cone flanks and the erosion of cinders into soil result in specific geomorphic modifications including a decrease in height, an increase in basal width, a decrease in crater depth and diameter, and a decrease in slope over time (Dohrenwend et al., 1986; Hooper and Sheridan, 1998; Wood, 1980b). The rate at which these modifications occur is dependent on climate (Hooper and Sheridan, 1998; Rech et al., 2001; Wood, 1980b). Wood (1980b) illuminated this point by contrasting the deep gullies and mature vegetation on the flanks of Volcan, erupted in 1937 in tropical Papua New Guinea (Simkin and Siebert, 1994) with the barren, un-gullied flanks of cones erupted approximately 50,000

years ago in the arid San Francisco volcanic field of Arizona. Hooper and Sheridan (1998) also made this connection when they hypothesized that the Springerville volcanic field has a higher erosion rate than the nearby San Francisco volcanic field because it receives more precipitation annually.

Climate not only affects the rate of erosion but also the type of erosion and mass wasting experienced by a cinder cone (Figure 5) (Fornaciai et al., 2012; Wood, 1980b). Computer models by Hooper and Sheridan (1998) demonstrate how various types of erosion each result in unique cone morphologies and rates of degradation. Rainsplash, soil creep, freeze-thaw, and bioturbation are linear diffusion processes. They are relatively slower processes and in the early stages of degradation, form convex hillsides. Overland flow and sheet was are non-linear and relatively faster erosion types. In computer models they form concave hillsides. Fornaciai et al. (2012)'s degradational models predict that cones eroded in very wet conditions might actually experience a decrease in basal width over time, as material is eroded from the cone summit and carried away by a robust fluvial system.

Chemical studies of cinder cone soils show that variations in temperature and insolation can affect the rate of soil development with higher temperatures and insolation correlating with faster soil development, increased amounts of vegetation and, as a result, higher hill slope stability (Rech et al., 2001). It is unknown if climate induced morphometric variations are identifiable within population-scale coarse resolution data sets.

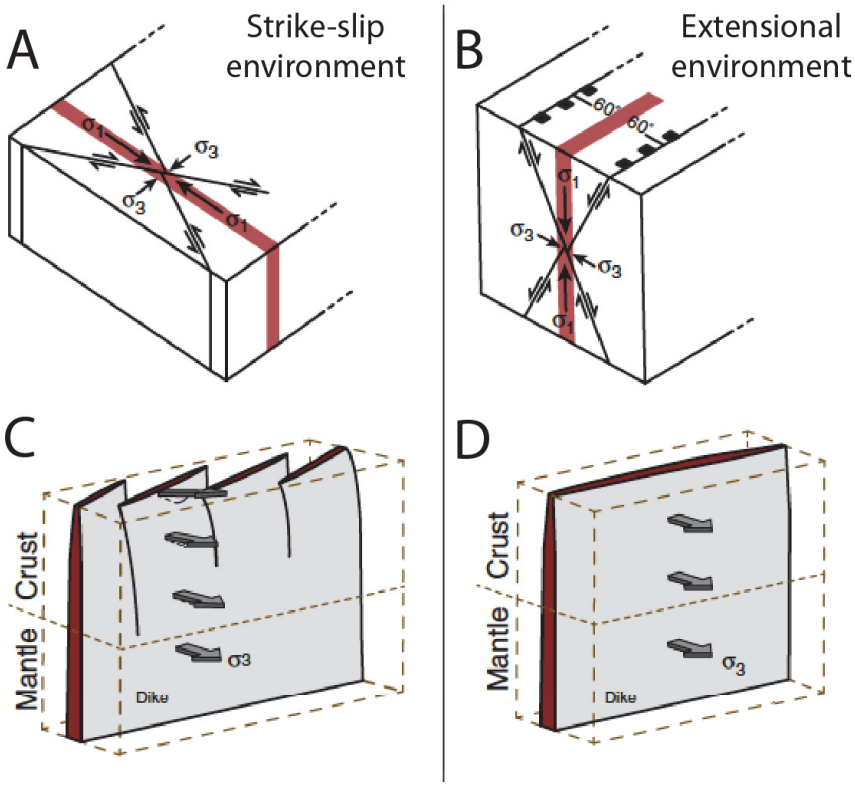

Figure 1: Top diagrams show the fundamental fault modes with stress tensors as σ1> σ2> σ3, after Anderson (1951). Magmatic intrusions are shown in red. A) Transform faults will form in a strike-slip environment (σ1 horizontal). B) Normal faults will form in an extensional environment (σ1 vertical). C and D) Dike orientations as a function of principle compressive stress. Image modified from Le Corvec et al. (2013b).

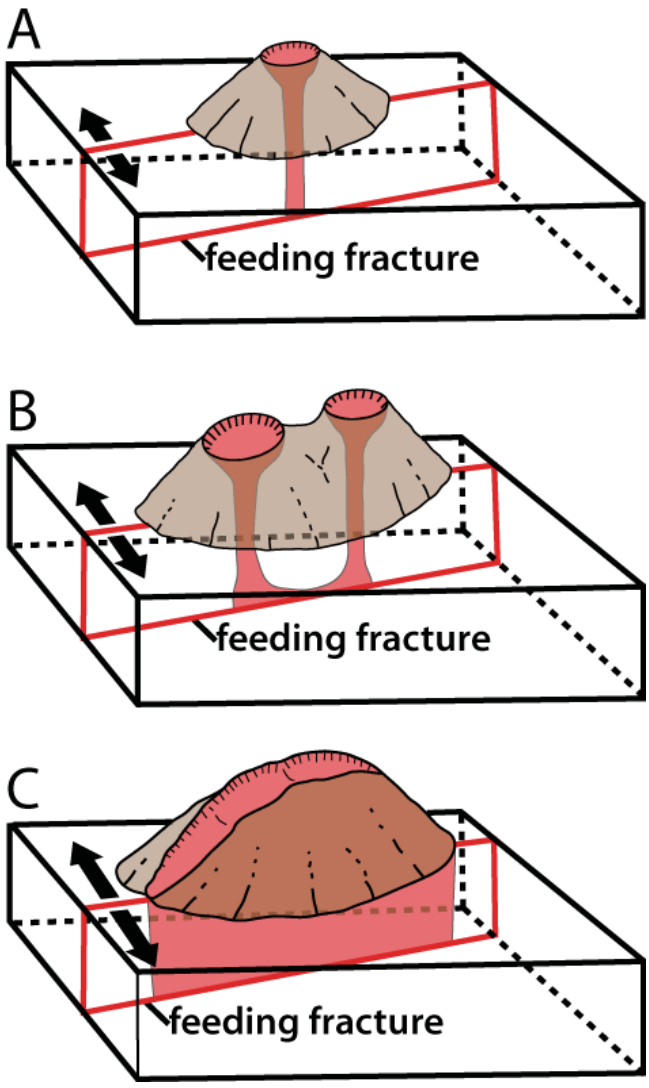

Figure 2: Schematic of cone classification scheme by Corazzato and Tibaldi (2006) based on morphology of coeval eruption points along a single magma-feeding fracture. Arrows indicate relative horizontal stress in extensional setting. A) Type 1 cone, erupted from single conduit from feeder dike. B) Type 2 cone, intermediate type. C) Type 5 cone: multiple rifted cone, strongly elongated and usually larger than other types. Formed along multiple eruption points from same feeder dike.

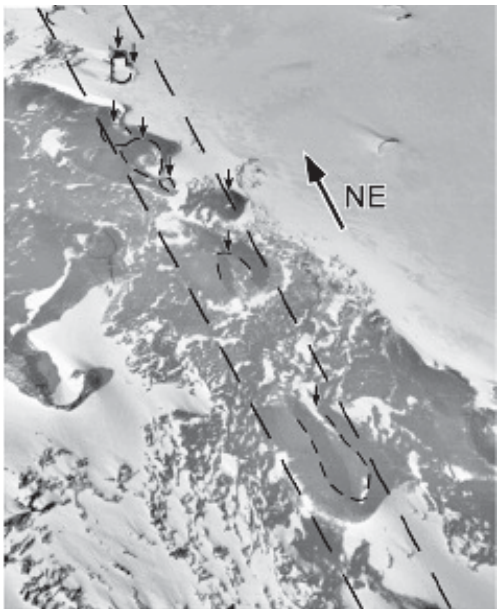

Figure 3: Aerial photograph of 6km long vent alignment on the Mount Morning shield, Antarctica. The long axes of craters indicate feeder dike orientation. The long dashed lines represent the underlying dike. The alignment of craters along the long axis trend of each other suggests they erupted from the same dike. Image modified from Paulsen and Wilson, 2010

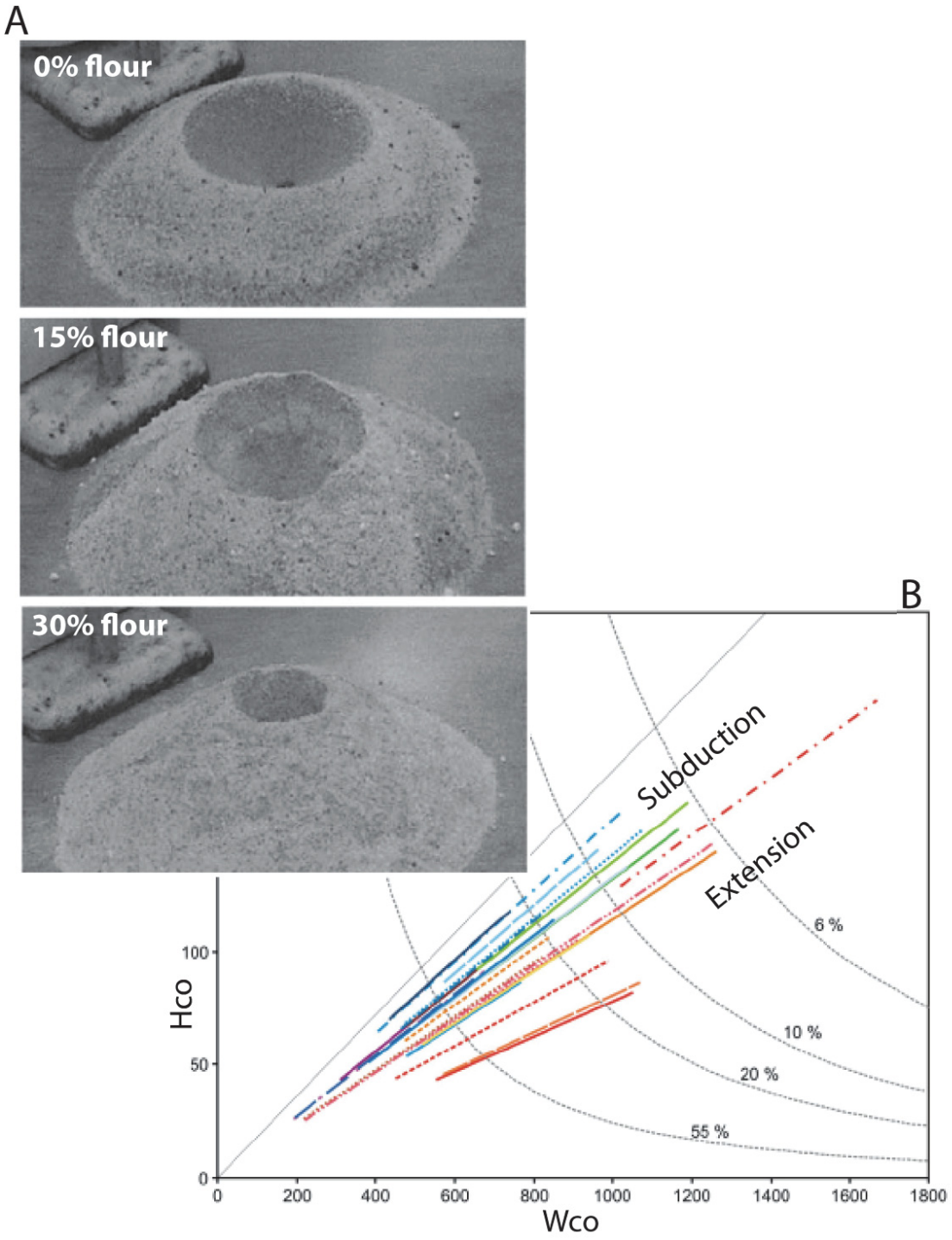

Figure 4: A) Sand models by Riedel et al., 2003 that highlight the effect of increasing the proportion of fine cohesive material (flour versus sand) on cinder cone morphology. B) Graph of cone height versus basal width from Fornaciai et al., 2012. Reddish tones correspond to rift-related cones; blue tones correspond to subduction-related cones.

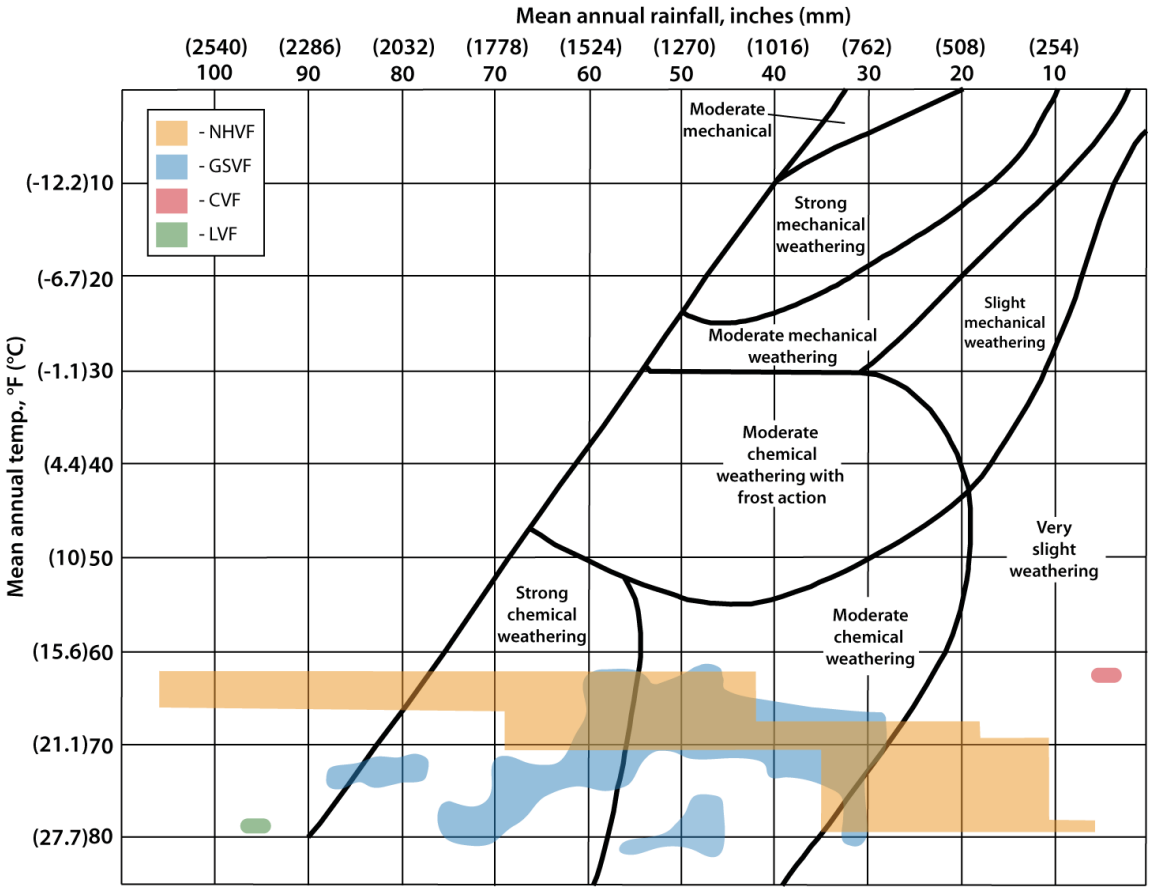

Figure 5: Climate process diagram from Peltier (1950) illustrating the types of weathering found in specific climatic settings. NHVF – Nyambeni Hills volcanic field, GSVF – Guatemalan Salvadorian volcanic field, CVF – Cima volcanic field, LVF- Lamongan volcanic field. The NHVF and GSVF are large volcanic fields that experience internal climate variability. The wettest side of the NHVF is in the south and the dry end is to the north. In the GSVF wetter cones are located in the West and drier cones are located to the East.

Study Sites

The Nyambeni Hills Volcanic Field

Situated approximately 200 km east of the Kenyan segment of the East African Rift System (EARS), the Nyambeni Hills volcanic field (NHVF) is one of 4 off-axis volcanic fields centered at 38° longitude (Figure 6). Stratigraphic studies and K-Ar ages indicate that the field underwent two stages of activity (Brotzu et al., 1984). The first began 4.5 Ma and was dominated by fissure eruptions of basanites, tephrites, and hawaiites (Brotzu et al., 1983). This stage ended approximately 2.9 Ma. Activity resumed at approximately 2.1 Ma, switching to more centralized cinder cone and maar forming eruptions. Activity has continued until recent times. The youngest radiometric age from the NHVF is 0.46 Ma (Opdyke et al., 2010).

All four volcanic fields of the Kenyan segment of the EARS are located on topographically elevated, blister shaped mini-domes. The term mini-dome is merely descriptive and does not have a genetic connotation. The prefix mini- has been added to give a sense of the relative scale of each dome compared to the much larger Ethiopian and Kenyan domes. It is unclear if the mini-domes formed due to an uneven volcanic pile or because of thermal uplift. Three off axis mini-domes, including the NHVF, display a strong NE-SW trend (Figure 6). Cones in the NHVF are concentrated along the crest of the mini-dome. The highest elevation in the NHVF is in the south. This region is the wettest and coolest (average annual precipitation about 1900 mm and average annual temperature approximately 19° C, (Sombroek et al., 1982)). The elevation and average annual precipitation decreases

progressively northward (Figure 7). Precipitation and temperature stratification with in the NHVF is caused by the blocking of prevailing SE winds by the southern crest of the mini-dome (Kamau et al., 2010). We believe that despite climate fluctuations over the past 2 Ma, the sharp climate delineation between the north and south sections of the Nyambeni hills is a persistent feature because it is caused by longstanding topography. The Köppen-Geiger classification of the NHVF is tropical-savannah (Aw) (Peel, et al., 2007).

Volcanism in the NHVF is associated with the EARS. Although still debated, analogue experiments, fault kinematic data, earthquake focal mechanisms, GPS, and fault characteristics support the existence of an E-W extensional regime. It remains unclear why any of the off axis volcanic fields, including the NHVF, display trends oblique to regional extension. The crust beneath the Nyambeni range shows no evidence of thinning, unlike the volcanically active rift grabens of the EARS (Maguire et al., 1994). The relationship between the Nyambeni Hills' magma source and axial volcanism remains unclear.

The Guatemalan Salvadorian Volcanic Field

The Guatemalan Salvadorian Volcanic Field (GSVF) encompasses the volcanic fields of Guatemala and El Salvador, including both the present volcanic arc and recent behind the arc volcanism. The back-arc region of the GSVF includes over 300 cinder cones, small shields, maars, and spatter cones, as well as a few major stratovolcanoes and large shields. The GSVF trends roughly parallel to the Central American volcanic front and began erupting approximately 1100 Ka to less than 50

Ka ago (Carr et al., 2003; Walker et al., 2011). The cinder cones are progressively younger towards the volcanic front. Although volcanism in the volcanic front is related to subduction, the back-arc portions of the GSVF are spatially associated with regional extension caused by the interaction of transform faults to the north and subduction-zone volcanism to the south (Burkart and Self, 1985; Guzmán-Speziale, 2001). The highest density of cinder cones in the GSVF is located in the NS trending Ipala Graben of southeastern Guatemala (Figure 8). In this study, we will refer specifically to the behind-the-arc cinder cones using the overall field name of GSVF for convenience and brevity.

Like the NHVF, the climate of the GSVF is diverse (Figure 5). Cinder cones located near the apex of the volcanic front receive the most moisture and are the coolest, averaging 2200 mm of precipitation annually with an average annual temperature of about 22.8 ° C (Schneider et al. 2011; INSIVUMEH, 2003). Cinder cones located behind the volcanic front or in the Ipala graben experience a drier climate and average about 800 mm of precipitation annually. The GSVF contains several Köppen-Geiger classifications including: tropical-monsoon (Am), temperate-dry winter-warm summer (Cwb), arid-steppe-hot (Bsh), and tropical-savannah (Aw) (Peel, et al., 2007).

Lamongan volcanic field

The Lamongan volcanic field (LVF) of East Java, Indonesia, is located on the flanks of the polygenetic volcano, Lamongan (Figure 9). It includes about 61 cinder or spatter cones and 27 maars (Carn, 2000). Volcanic activity at Lamongan is

caused by the subduction of the Indo-Australian plate beneath the Eurasian plate (Puspito and Shimazaki, 1995). The tectonic structure underlying Lamongan is not understood, although radar imagery shows evidence for approximately NW-SE and NE-SW faulting (Carn, 1999). There are no absolute ages available for any volcanic deposits on or around Lamongan. Both Lamongan and the surrounding parasitic cones are historically active; the last major eruption took place in 1889 (Simkin and Siebert, 1994). The Köppen-Geiger classification of Mount Lamongan is tropical-monsoon (Am) (Peel, et al., 2007). The average annual precipitation is 2413 mm and the average annual temperature is 26° C (Schneider et al. 2011).

Cima Volcanic Field

The Cima volcanic field (CVF) is located in the eastern Mojave Desert approximately 120 km southwest of Las Vegas, NV (Figure 10) It encompasses about 40 Pleistocene cinder cones and their associated lava flows. K-Ar dating reveals that the CVF has had three separate periods of volcanic activity ranging from the late Miocene through the latest Pliocene and that the locus of volcanic activity has moved southward over time (Dohrenwend et al., 1984). The tectonics of the CVF are complex, owing to its proximity to the Basin and Range and the San Andreas Fault system. Early Miocene extension was eventually replaced by a contractional tectonic regime (Bartley et al., 1990). The age of this change is unclear. The Köppen-Geiger classification of the CVF is arid-desert-hot (Bwh) (Peel, et al., 2007). The average annual temperature is 17° C and it receives an average of 149 mm of precipitation annually (Schneider et al., 2011).

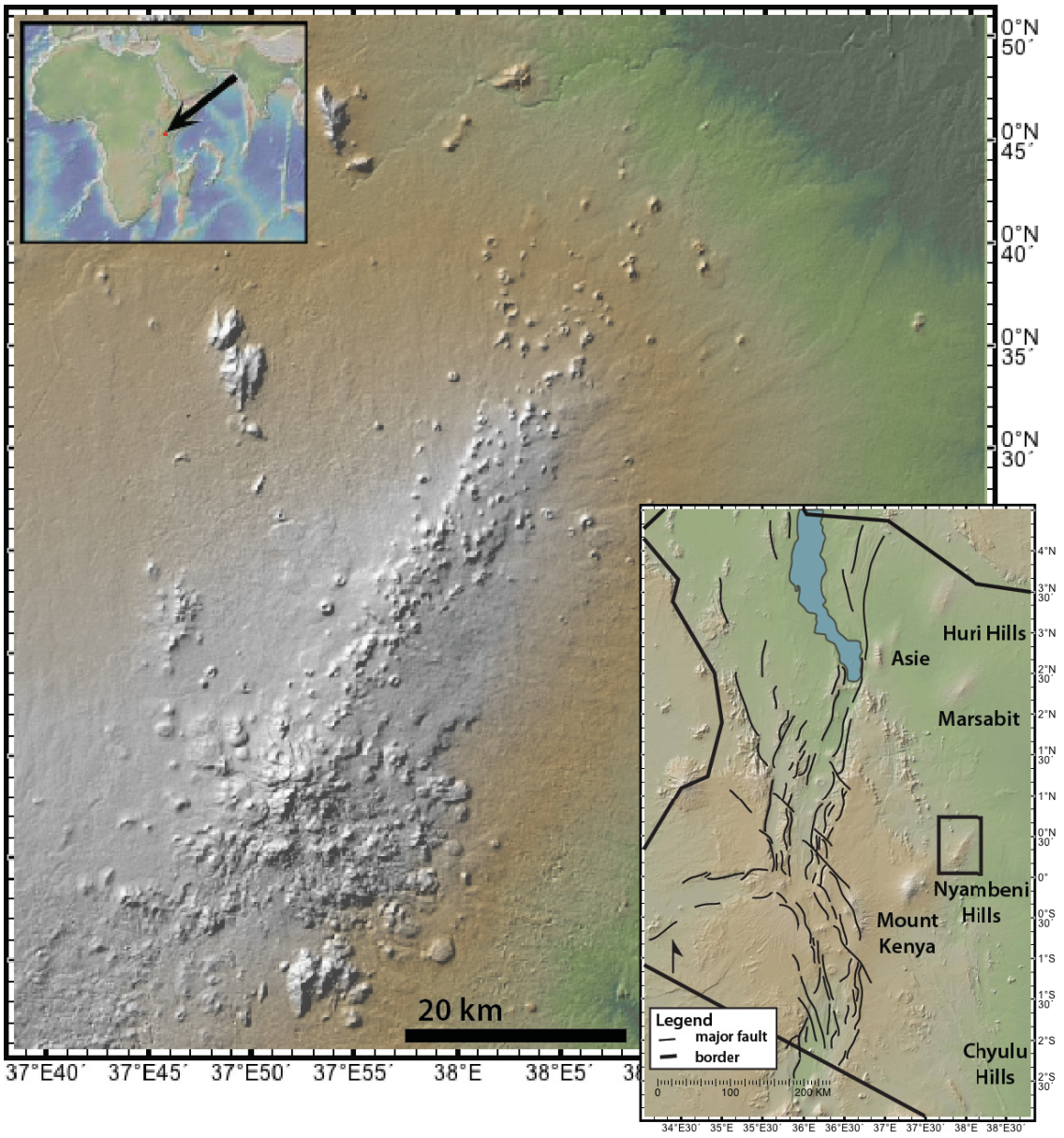

Figure 6: Digital elevation map of the Nyambeni Hills Volcanic field. Pull out shows the locations of major faults in the Kenyan section of the East African Rift System with respect to the study site. Note the NE trend of most off-axis volcanic fields, including Huri Hills, Marsabit, and Asie. Chyulu Hills volcanic field is oriented NW-SE. Faults on pull out after Smith (1994). Data accessed with GeoMapApp.

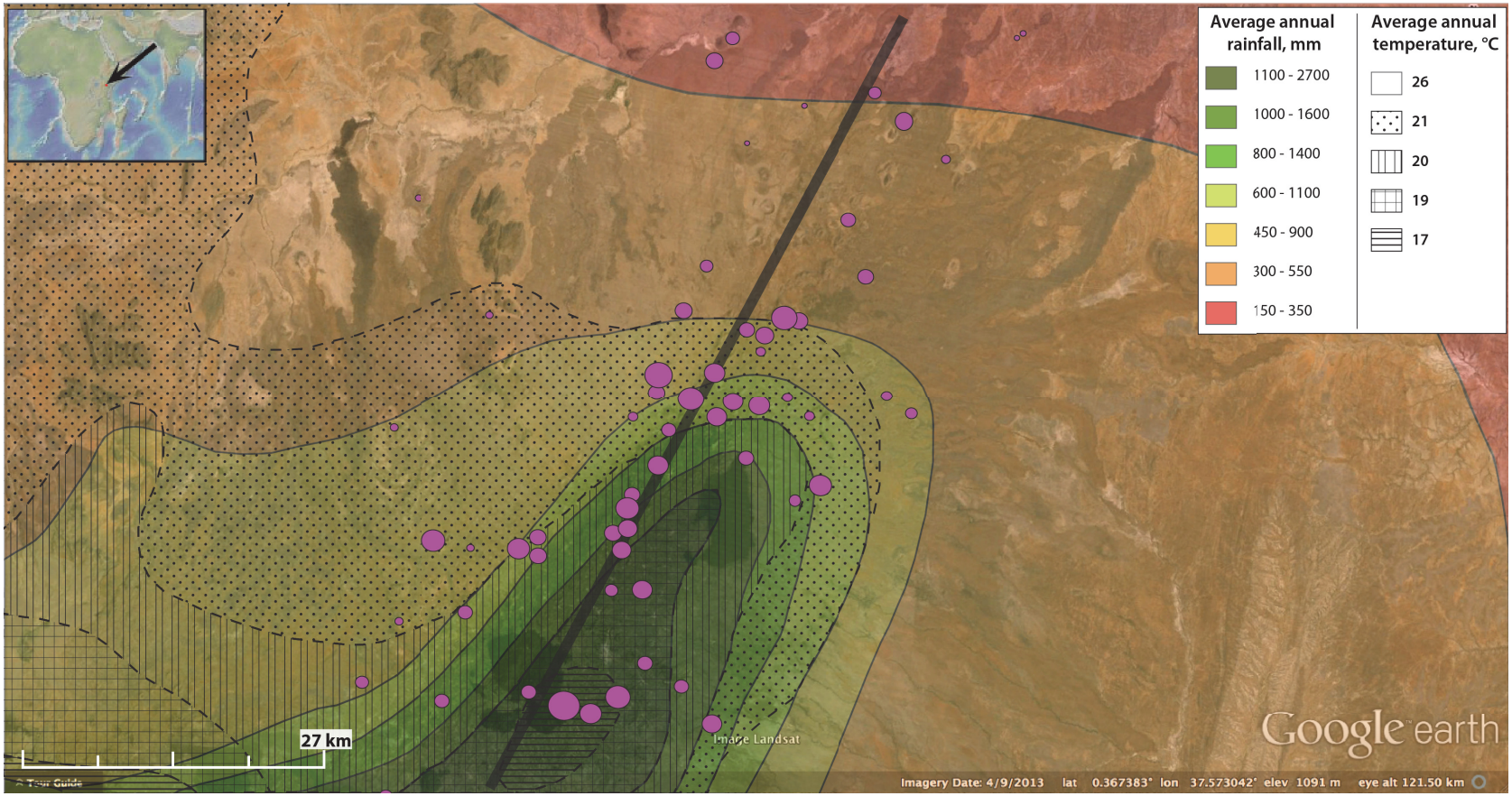

Figure 7: Satellite image of the NHVF overlain with climate zones. Black line represents mini-dome crest. Pink circles mark the location of measured cones. Circle size represents relative Hco/Wco values. Climate information from Sombroek et al., 1982

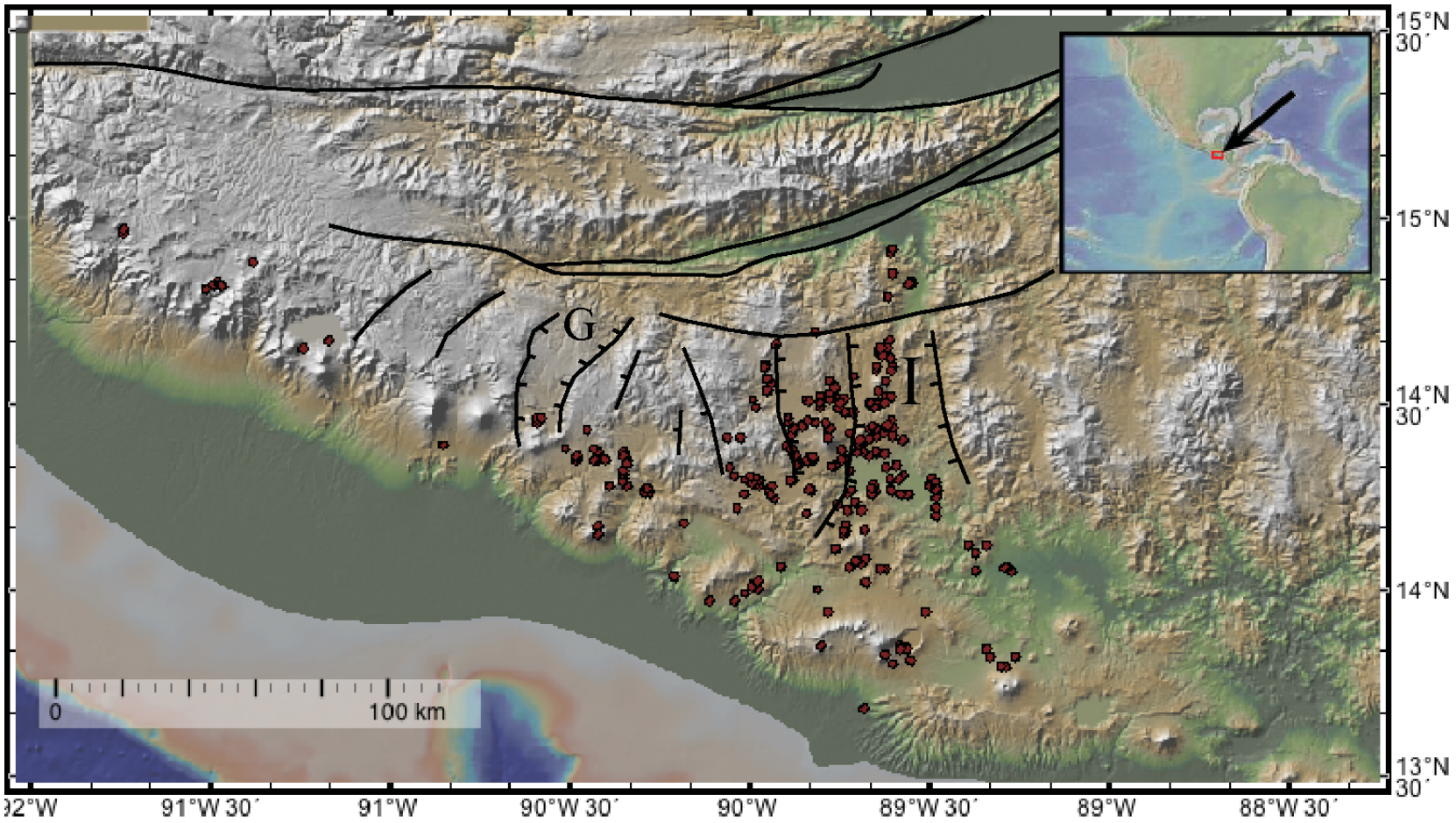

Figure 8: Digital elevation map of the Guatemala Salvadorian volcanic field. Circles represent location of cinder cones. Black lines are major faults, adapted from Lyon-Caen et al., 2006. Data accessed using GeoMapApp. I - Ipala Graben, G - Guatemala City graben

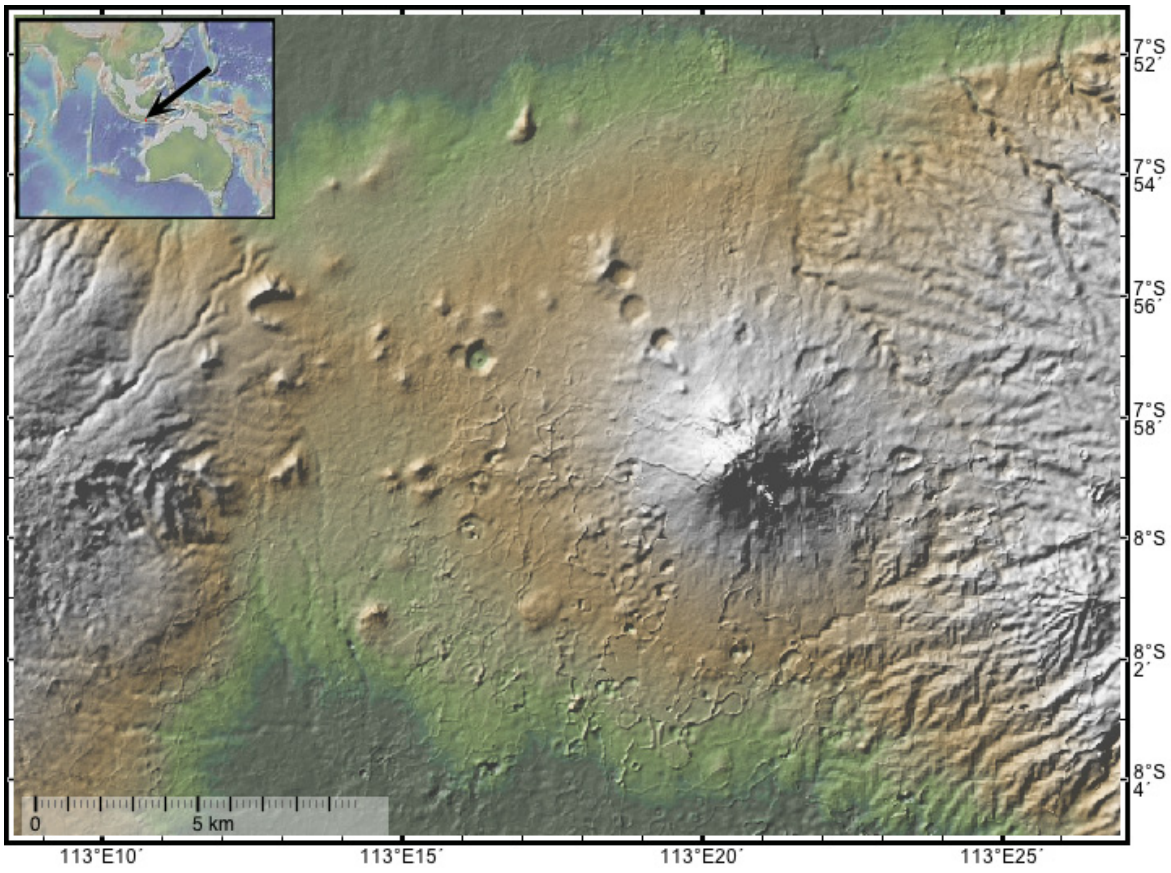

Figure 9: Digital elevation map of Lamongan volcanic field. Large cone in center is Mount Lamongan. Data accessed using GeoMapApp

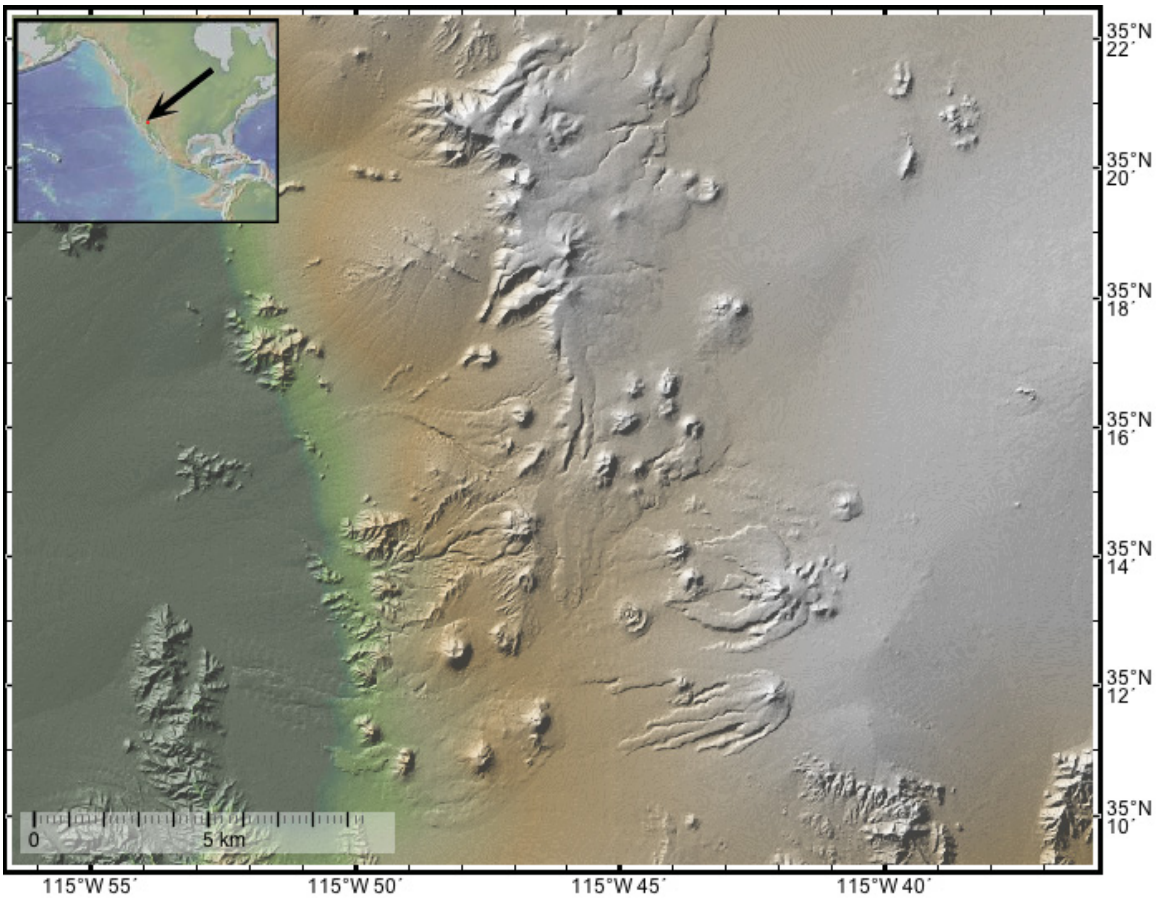

Figure 10: Digital elevation map of Cima volcanic field. To the immediate right is the Cima Dome. Data accessed using GeoMapApp

Table 1:
Summary of study site characteristics

	Location	Field type	N	Tectonic Setting	Average annual precipitation, mm	Average annual temperature, °F	Köppen – Geiger classification*	Age range	Latitude	Longitude
NHVF	Kenya	Volcanic field	64	Crustal Extension	150 - 2700	17 - 26	Aw	Pleistocene	0.1° N	37.8° E
GSVF	Guatemala, El Salvador	Mostly volcanic field***	254	Back-arc extension**	750 – 2200	17 – 27	Aw, Am, Cwb, Bsh	Mid-late Pleistocene	14.0° N	89.5° W
LVF	East Java, Indonesia	Parasitic, Stratovolcano	36	Volcanic arc	2413	26	Am	Pleistocene – recent	7.98° S	113.34° E
CVF	California, USA	Volcanic field	11	Crustal Extension	149	17	Bwh	Late Miocene - Pleistocene	35.2° N	115.8° W

* See reference (Peel et al., 2007) for more information on classifications
**The cinder cones in this study are largely in the back arc. The GSVF more broadly includes the front arc as well.
*** The back-arc region of the Ipala Graben is a volcanic field in type. Some individual cones, especially near the volcanic front, are parasitic to stratovolcanoes.

METHODS

Morphological Measurements

Following protocols established by earlier studies (Dohrenwend et al., 1986; Hasenaka and Carmichael, 1985b; Porter, 1972; Wood, 1980b) I characterized cinder cone morphology by measuring basal diameter (Wco), cone height (Hco), and crater width (Wcr). Morphological measurements of the NHVF are all original to this study. I utilized a combination of publically available satellite imagery and ASTER GDEM. I made four cross sections per cone, centered in the middle of the crater or at the summit when there was no crater, and drawn at approximately every 45° (Figure 11). The basal diameter was visually identified based on a break in slope and averaged across the four cross sections to account for ellipticity (Figure 11). Height was defined using the Porter (1972) method, as the maximum difference between the average basal elevation and the crater rim or summit. This method is suitable for the NHVF because the average basal slope is less than 5° (Massimiliano Favalli and Pareschi, 2004). Crater widths were also visually identified and averaged across the four cross sections.

Slope was not measured directly but calculated as an average value using formulas developed by Hooper and Sheridan (1998). For cones with a crater the formula is

$$S_{avg} = tan^{-1}\left(\frac{2H_{co}}{W_{co} - W_{cr}}\right)$$

where Savg is the average slope of the cone flanks, Hco is the cone height as defined in Porter (1972) and Wco is the average basal diameter. For cones without craters where Wcr = 0, the formula reduces to

$$S_{avg} = tan^{-1}\left(\frac{2H_{co}}{W_{co}}\right)$$

Volumes were calculated as a maximum value without subtracting the volume of an associated crater using the formula

$$V = \frac{1}{3}\pi R_{co} H_{co}$$

where Rco is the basal cone radius, defined as half of Wco.

I measured additional morphometric parameters in the NHVF including crater ellipticity and the azimuth of crater elongation on 372 craters visible from satellite images at a resolution of 3:5000. A small fraction of craters are associated with maars, fissures, or complex cones; the vast majority of craters are associated with cinder cones. I included all craters because the distribution of volcanic vents at the surface is indicative of feeder dike orientation. To measure the craters, I layered satellite images on top of ASTER GDEMs and manually traced visibly identifiable craters. After tracing the craters I ran them through a Matlab based, best-fit ellipse program inspired by work of Paulsen and Wilson (2010). The Matlab program was created in collaboration with Niki Yoshiuchi, affiliated with New York University Polytechnic School of Engineering, and is available for download at (http://github.com/aplusbi/ellipse). This program creates a best-fit ellipse around each crater trace and then provides the length of the long and short axes of each

best-fit ellipse, as well as the orientation of the long axis (Figure 12). I used the axial ratio of the best-fit ellipses, defined as the minor axis divided by the major axis, as a proxy for cone ellipticity. To measure the orientation of the entire volcanic field I used Le Corvec et al., (2013b)'s method by creating a convex hull around the NHVF and fitting it with a best-fit ellipse. The long axis of the best-fit ellipse provides a sense of the orientation of the whole volcanic field.

Morphological data from the CVF, LVF, and GSVF were taken from literature (Bemis et al., 2011; Carn, 2000; Dohrenwend et al., 1986). Those studies report similar definitions and measurement approaches for cinder cone morphology. Slope and volume were recalculated using the given equations for consistency across the four study sites. Data for the CVF was obtained from 1:24,000 topographic maps with 10 m contours and spot-checked by fieldwork. Carn (2000) used 1:50,000 maps to measure cones in the LVF. Morphological data for the GSVF was measured using topographic maps at a scale of 1:50,000 with a contour interval of 20m. Maars and composite cones were removed from all data sets by limiting the minimum and maximum height and by visual identification.

Error

The geomorphological measurements used in this study come from a variety of topographic maps and digital sources. For this reason there is variability in the measurement errors between each volcanic field. Error estimates for the GSVF and LVF are 10-20 m for cone height and 50-100 m for basal width. This results in a mean error of approximately ± 0.06 in Hco/Wco and ± 0.22 in Wcr/Wco for the

GSVF and ±0.05 Hco/Wco and ±0.16 Wcr/Wco for the LVF. The CVF has an error estimate of 5-10 m for height and 25-50 m for basal width and a corresponding mean Hco/Wco error of ± 0.03 and a mean Wcr/Wco error of ± 0.12. The NHVF data was measured from ASTER GDEMs at a scale of 30 m and with a vertical error of ± 7.4 m and a horizontal error of 82 m (Meyer et al., 2012). This results in a mean Hco/Wco error of ± 0.02 and a mean Wcr/Wco error of ± 0.11.

Error estimates of Hco/Wco and Wcr/Wco are inversely proportional to cone size with smaller cones having the greatest error and larger cones having lower errors. Fornaciai et al. (2012) cautions against the use of topographic data with a resolution equal to or less than ASTER GDEMs for cones with a volume $<30 \times 10^6$ m^3 because morphological measurement errors can be in excess of 20% when compared to 2m resolution LIDAR data. For cones smaller than $<30 \times 10^6$ m^3 they suggest using topographic information at a resolution of 10 m or less. Unfortunately, publically available topographic maps and DEMs of Kenya, Guatemala, El Salvador, and Indonesia generally have limited resolution. Higher resolution data are either not available or prohibitively expensive.

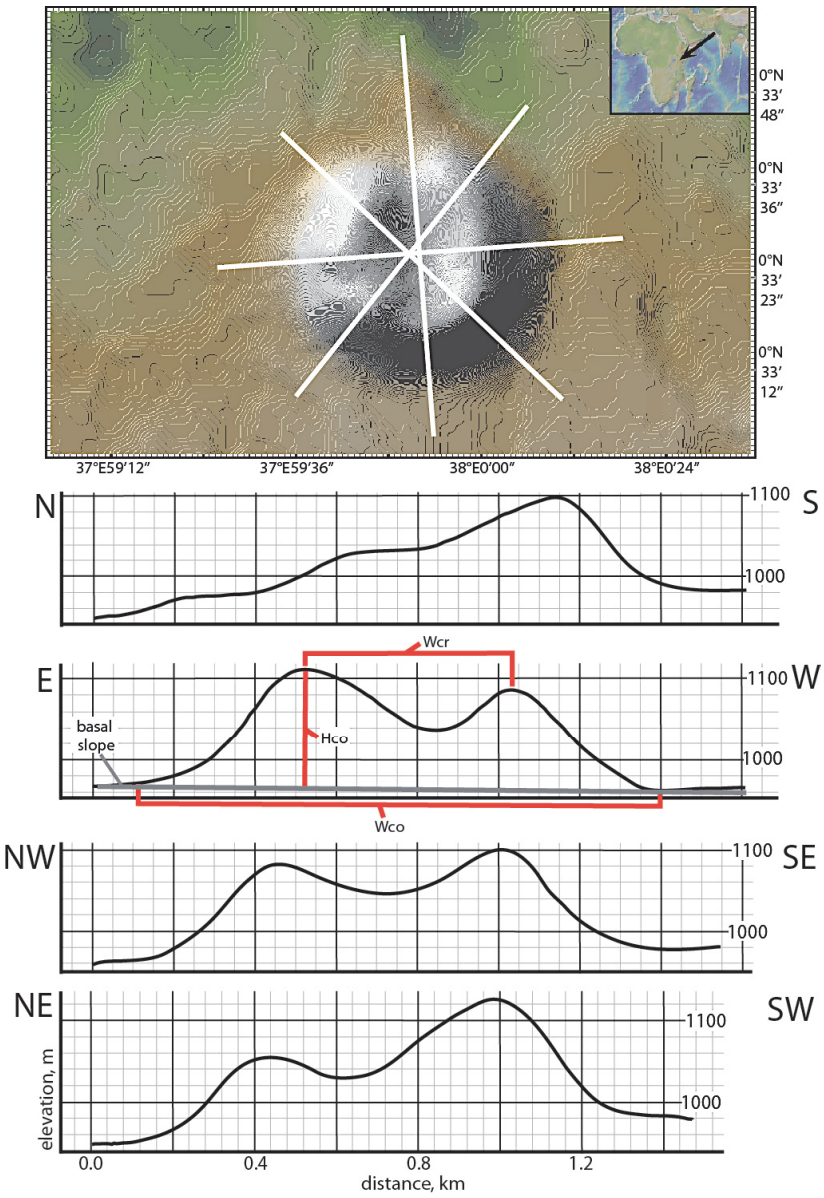

Figure 11: Cone detailing morphological definitions and measurement method. Basal width (Wco) and crater width (Wcr) were averaged across four cross sections. I used the maximum cone height for Hco.

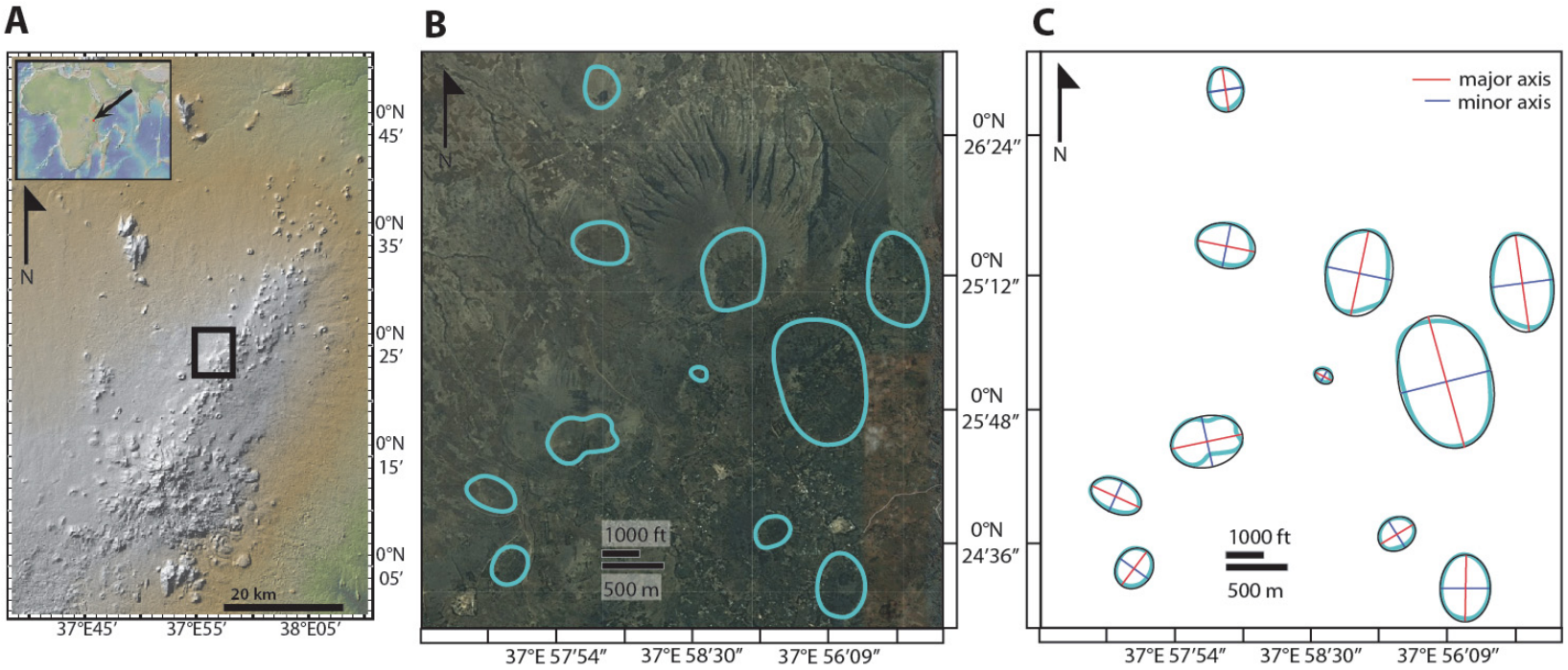

Figure 12: A) Digital elevation map of NHVF. Box shows location of B and C. B) Satellite image with manually drawn crater traces. Crater rims were identified visually based on a combination of elevation changes and surface texture patterns. Draping satellite imagery on digital elevation maps highlighted these characteristics. C) Output of best-fit ellipse program. Azimuth of elongation is represented by major axis. Axial ratio is defined as minor axis/major axis.

RESULTS

Cone Morphologies

The morphometric parameters of 367 cones from four volcanic fields ranging in climate from tropical to arid are summarized in Figure 13 and Table 2. The cinder cones display a large range in size and shape. The average values for each field also have substantial differences.

As mentioned in the Background, Fornaciai et al. (2012)'s morphometric analysis found that cones associated with subduction arcs are larger, steeper and have lower Wcr/Wco values than intraplate ones. They attributed these differences to variations in eruption dynamics. Here we see both consistent and inconsistent differences between the volcanic fields and their tectonic setting (Table 2). The NHVF and CVF are both intraplate fields associated with rifting. Although the CVF contains the smallest cinder cones, the NHVF contains the largest. Both the CVF and NHVF have high Wcr/Wco values, 0.43 and 0.37 respectively, which are above or very close to the ideal Wcr/Wco value for unmodified cones of 0.40, and higher than the values for the GSVF (subduction/rifting) and the LVF (subduction). These relationships are consistent with Fornaciai et al. (2012)'s findings. The higher than ideal Wcr/Wco value in the NHVF might relate to the average diameter or height of the magma conduit within in the cones. Kervyn et al. (2012) obtains higher than ideal Wcr/Wco values in sand experiments by increasing the conduit diameter and/or height. These changes also cause a drop in Hco/Wco. This pattern is similar to what we observe in the NHVF suggesting that the magma conduits there might be, on average, wider or higher than the other fields.

Slopes in the NHVF and CVF are relatively high (21° and 25° respectively) compared to the GSVF and LVF, although all four fields have lower slopes, on average, than the ideal value of 33°. This is inconsistent with Fornaciai et al. (2012)'s observations, but still unsurprising since only the LVF contains historically erupted, and therefore, possibly unmodified cones. The fact that the CVF has the highest slopes might result from the field experiencing relatively slow erosion rates due to the arid climate. The CVF not only has the highest slopes but also the highest Hco/Wco value, 0.16, consistent with the hypothesis that it has experienced less erosion than the other fields because it is closest to the unmodified ideal value of 0.18.

The GSVF and LVF are both associated with volcanic arcs. The LVF is the only field that contains cones < 200 years old and, for this reason, we would expect it to more closely resemble ideal values. This is not the case. The LVF has the lowest mean Wcr/Wco. (0.2), the lowest average slopes (16°), and a very low mean Hco/Wco (0.13). Cones in the LVF are neither relatively large nor steep like Fornaciai et al. (2012) predicts. Additionally, all the LVF morphometric averages are lower than expected for young unmodified cones. The simplest (and most traditional) hypothesis is that cones in the LVF have experienced relatively rapid erosion due to the tropical-monsoon climate but this is impossible to confirm without radiometric ages (Wood, 1980b; Hooper and Sheridan, 1998).

The GSVF displays characteristics of both intraplate cones and arc related cones. The average Wcr/Wco in the GSVF is high (0.35) and cones are relatively small, both characteristics of intraplate cones, but the slopes are relatively steep

(22°) and the average Hco/Wco is high (0.15) as expected for subduction related cinder cones.

Morphology and cone distribution within the NHVF

The NHVF, like other off axis-volcanic fields of the Kenyan section of the EARS, sits atop an NE trending ellipsoid mini-dome characterized by elevated topography. The morphometric parameters of 65 sampled cones change systematically moving E or W away from the crest of the mini-dome (Figure 7). The average slope and Hco/Wco ratio both decrease moving E or W from the crest (Figure 14). Examining Hco/Wco more carefully, we can see that ratio's decrease is caused by a progressive decrease in cone height (Figure 14). The range in basal width does not change moving away from the crest. The decrease in height is coupled with a progressive decrease in volume E or W of the crest.

Using the methods described earlier, I identified, traced, and processed 379 craters from the NHVF (Figure 15). Figure 16 contains summary statistics and frequency distribution of axial ratio and azimuth of elongation data from the NHVF and the GSVF. The mean axial ratio for craters in the NHVF is lower than the GSVF (0.74 versus 0.81). This means on average, cones in the NHVF are more elongated than those in the GSVF. The frequency distribution of craters with axial ratios > 0.6 is similar between the two fields. Differences arise on the lower end of the axial ratio spectrum. In the GSVF there are nearly zero craters with an axial ratio below 0.6. The NHVF, on the other hand, contains craters with axial ratios as low as 0.2. The mean axial ratio of the NHVF is consistent with other normal extensional systems,

falling between the Ethiopian Rift and Tepic Rift (mean axial ratios 0.77 and 0.66 respectively (Tibaldi, 1995).

Crater azimuths of elongation in the NHVF preserve a NNW to NNE signal (Figure 16). The most elongated 50% of craters (axial ratio < 0.76) preserve a strong NNE signal. The orientation of elongated craters does not trend as NE as the overall cinder cone population (Figure 15).

Table 2:
Summary of morphometric parameters of four study sites and ideal unmodified cone.

Field	N	Wco, m	Std. dev.*	Hco, m	Std. dev.	Hco/ Wco	Std. dev.	Slope	Std. dev.	Volume (10^6 m^3)	Std. dev.	Wcr/ Wco	Std. dev.
NHVF	64	1037	*357*	133	*63*	0.13	*0.04*	21°	*8*	74	*74*	0.43	*0.22*
GSVF	254	657	*267*	101	*49*	0.15	*0.04*	22°	*7*	23	*27*	0.35	*0.11*
LVF	36	760	*467*	94	*57*	0.13	*0.03*	16°	*6*	32	*54*	0.2	*0.01*
CVF	11	597	*138*	95	*29*	0.16	*0.02*	25°	*6*	15	*14*	0.37	*0.08*
ALL	365	732	*337*	106	*54*	0.15	*0.04*	21°	*7*	32	*46*	0.35	*0.12*
Ideal	n/a	n/a	*n/a*	n/a	*n/a*	0.18	*n/a*	33°	*n/a*	n/a	*n/a*	0.4	*n/a*

*Std. dev. = standard deviation

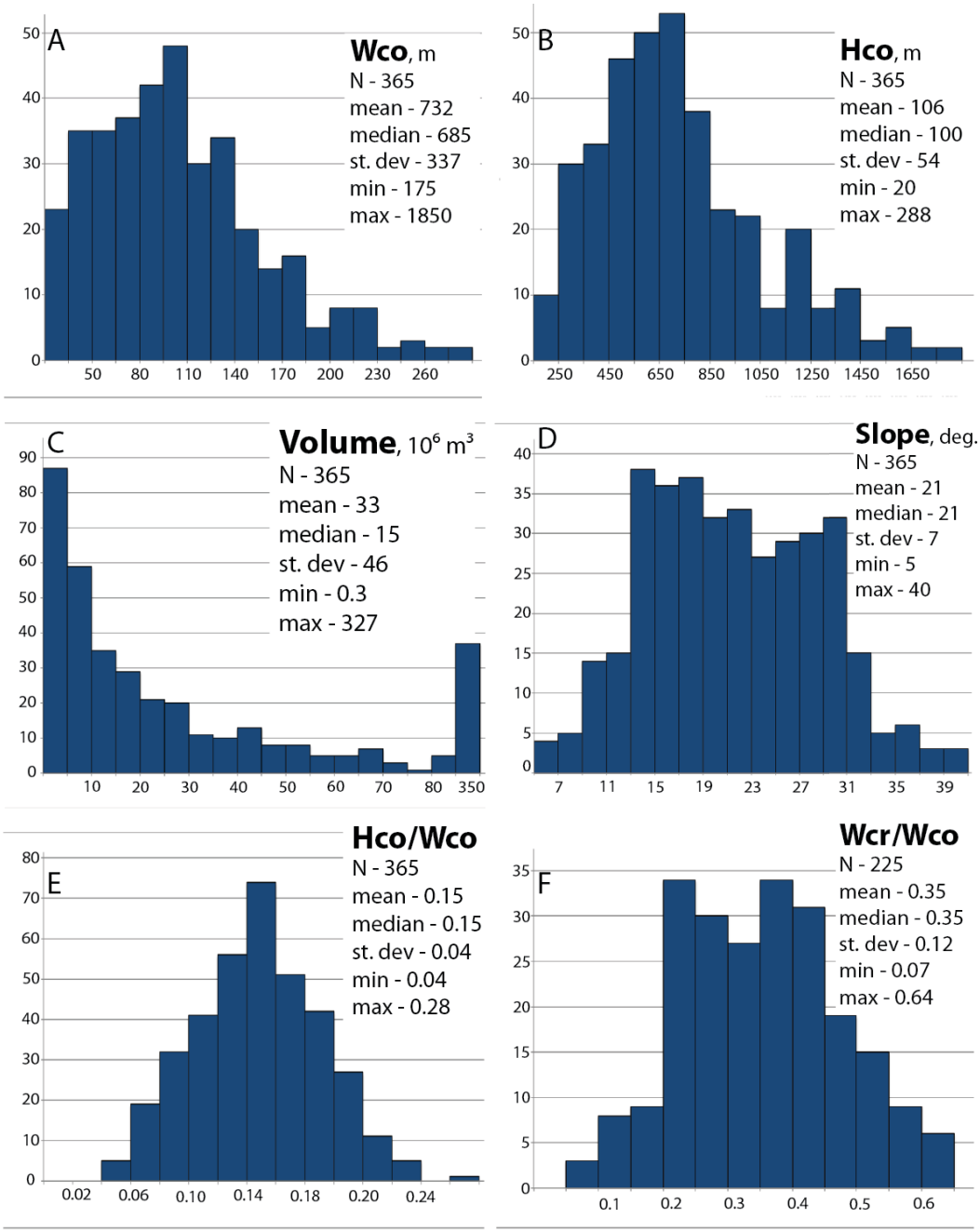

Figure 13: Frequency distributions of A) Basal width B) Cone height C) Volume D) Slope E) Hco/Wco F) Wcr/Wco Descriptive statistics are given for each morphometric measurement. N = number of cones, St. Dev. = standard deviation.

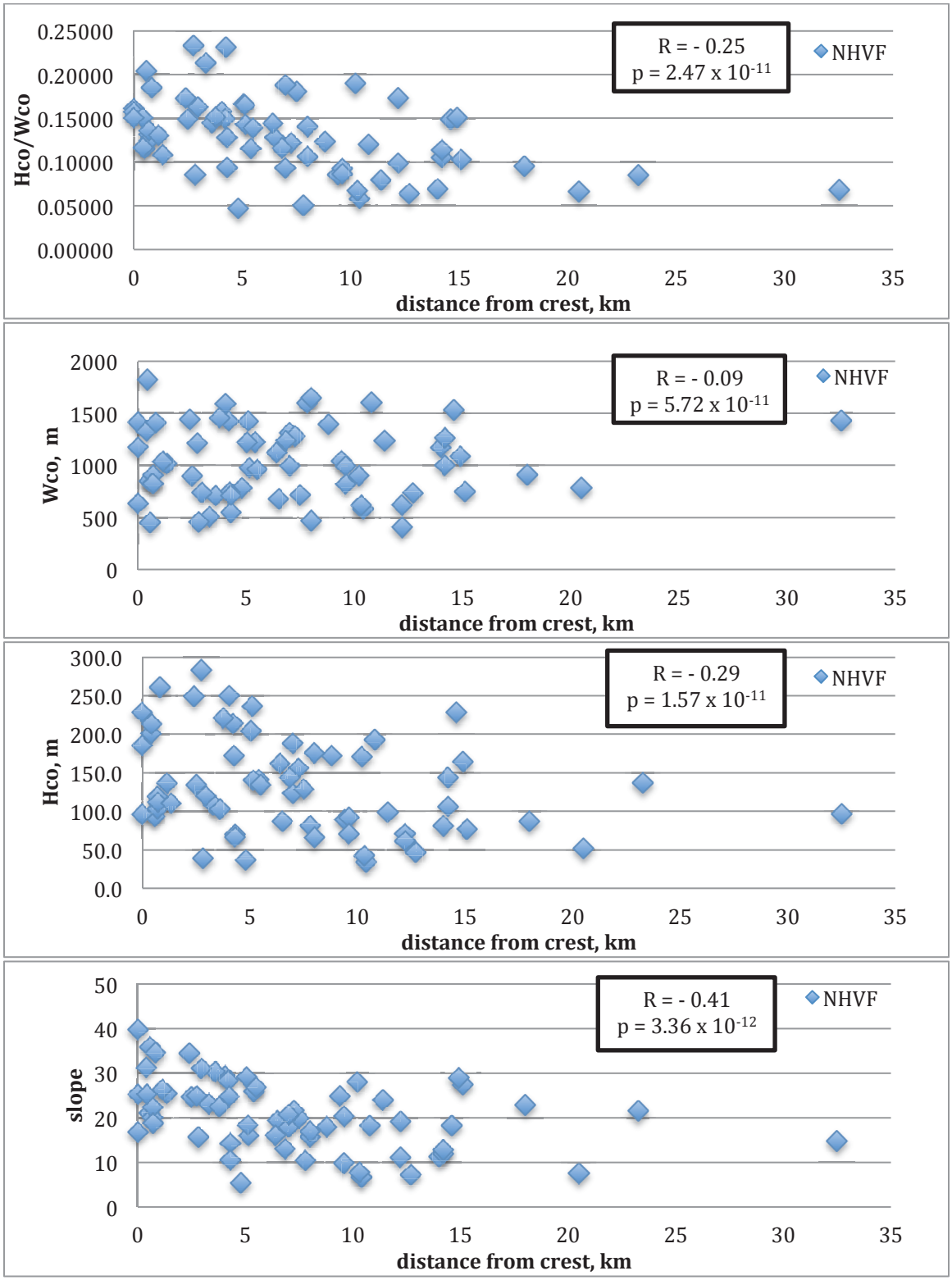

Figure 14: Morphometric parameters in relation to distance from mini-dome crest. A) Cone height-to-basal width ratio B) Basal width C) Cone height D) Slope in degrees

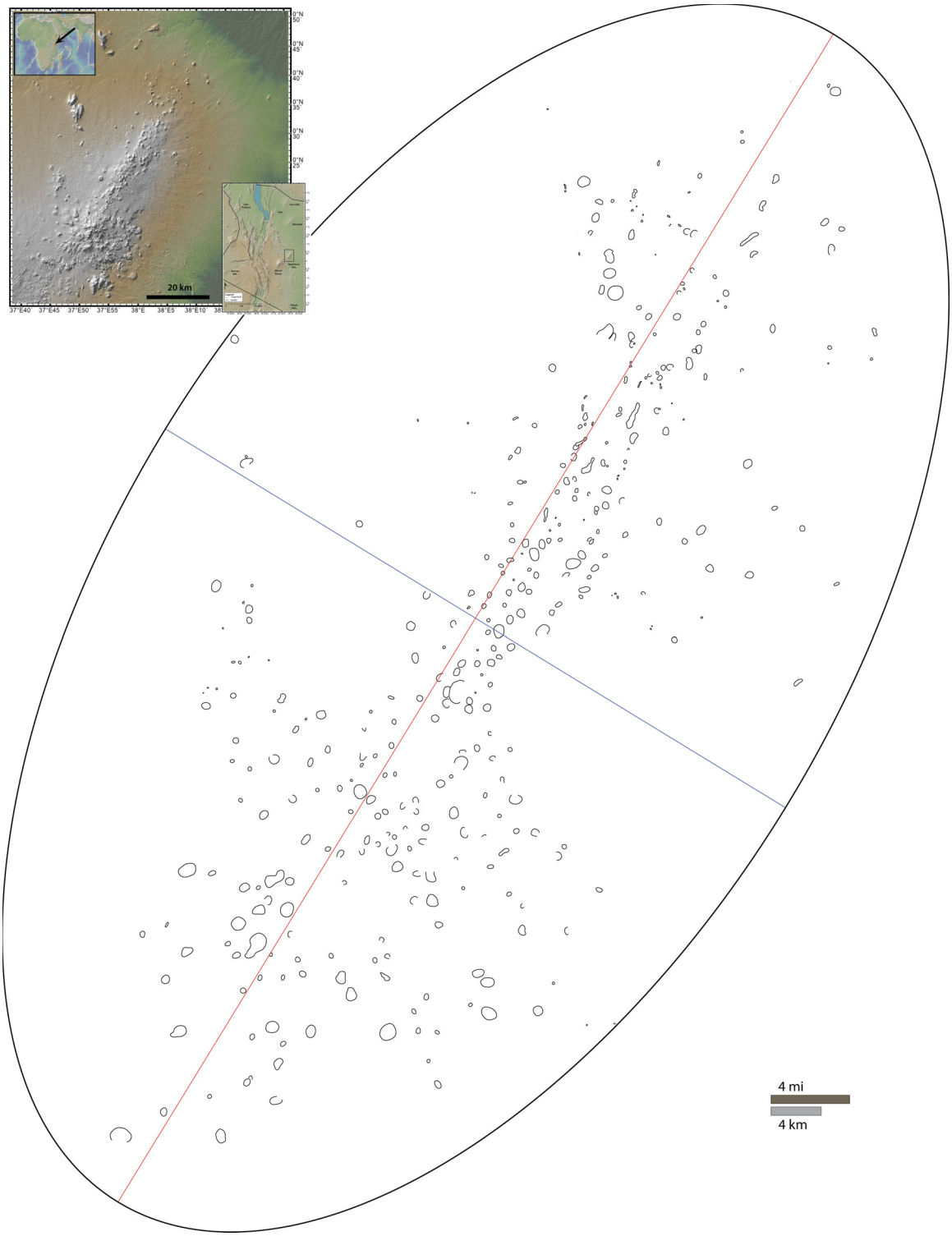

Figure 15: Craters of the Nyambeni Hills volcanic field. Large ellipse represents best-fit ellipse fitted to convex hull of entire field. Major axis is red and minor axis is blue.

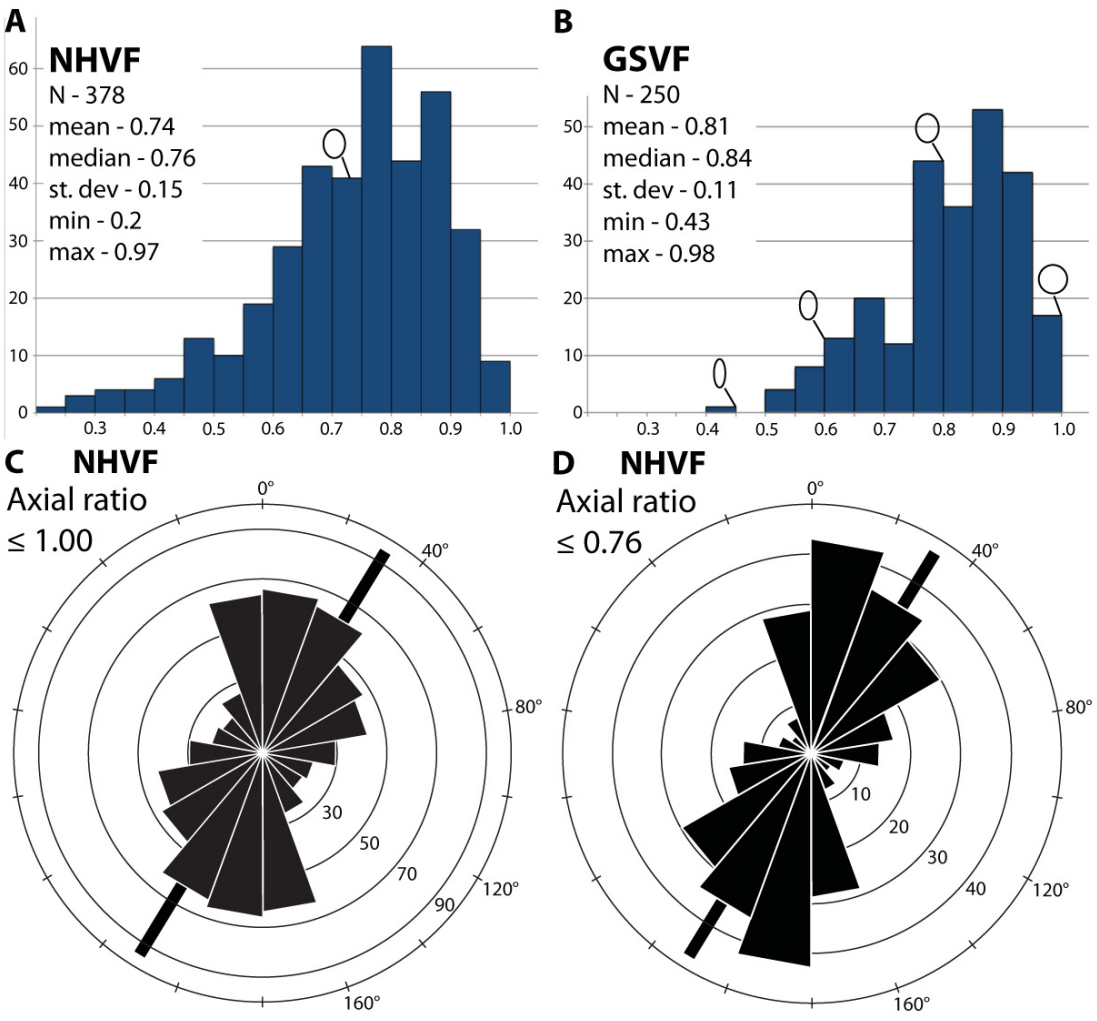

Figure 16: A) Summary statistics and frequency distribution of axial ratio data from the NHVF. Circle indicates the shape and location of the axial ratio 0.76. B) Summary statistics and frequency distribution of axial ratio data from the GSVF. Circles show shape and location of various axial ratios. C) Rose diagram of azimuths of elongation for all craters in the NHVF D) Rose diagram of azimuths of elongation for craters with axial ratio of 0.76 or less. Represents 50% of craters. Rectangle in C and D gives the azimuth of elongation for the entire field.

Climate and cinder cone morphology

Regardless of climate type (arid, temperate, or wet), each volcanic field has a wide range of values for basal diameter, cone height and slope. This is true even in fields with internal climate diversity like the GSVF and the NHVF (Figure 17-20). In the GSVF, Hco/Wco values narrow towards the mean when moving from dry to wet areas. In the NHVF, Hco/Wco is highest in temperate and very wet areas. A closer examination of Hco/Wco in the NHVF reveals a slight increase of basal width in wet areas coupled with a steeper increase in cone height. The range in height and basal width does not change between climate types in the GSVF. The range in slope is constant between wet and dry areas of the GSVF; however, in the NHVF slopes increase from arid to temperate climates and then steeply drop off in the wettest zones.

In the NHVF climate is strongly correlated with latitude (Figure 21). As a result, another way to identify climate based morphological trends in the NHVF is to plot morphological parameters against latitude. In all cases, correlations between latitude and morphology are very weak (Figure 21).

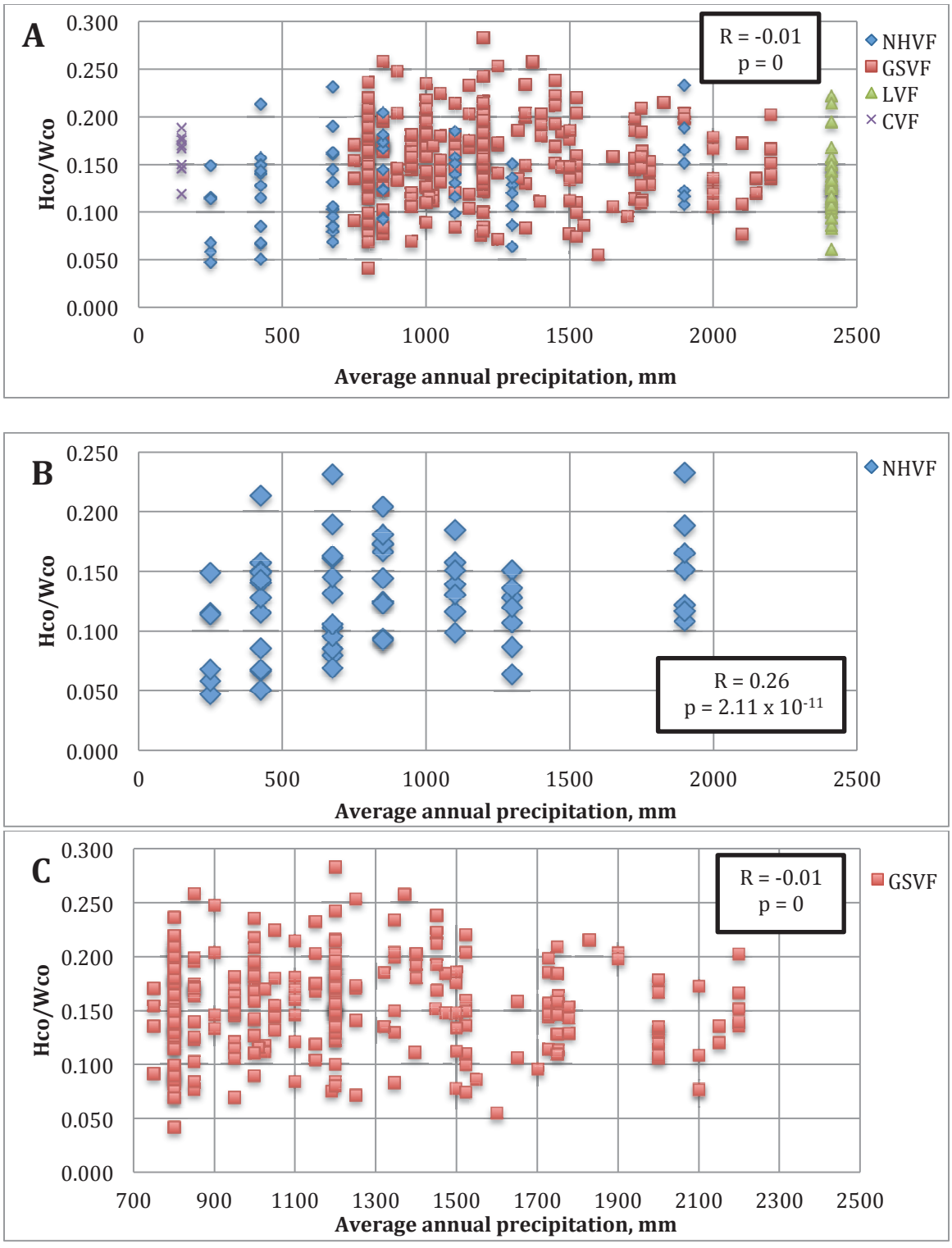

Figure 17: Summary of Hco/Wco in relation to the average annual precipitation. A) Hco/Wco of all study sites versus average annual precipitation. B) Hco/Wco of the NHVF versus average annual precipitation. C) Hco/Wco of GSVF versus average annual precipitation.

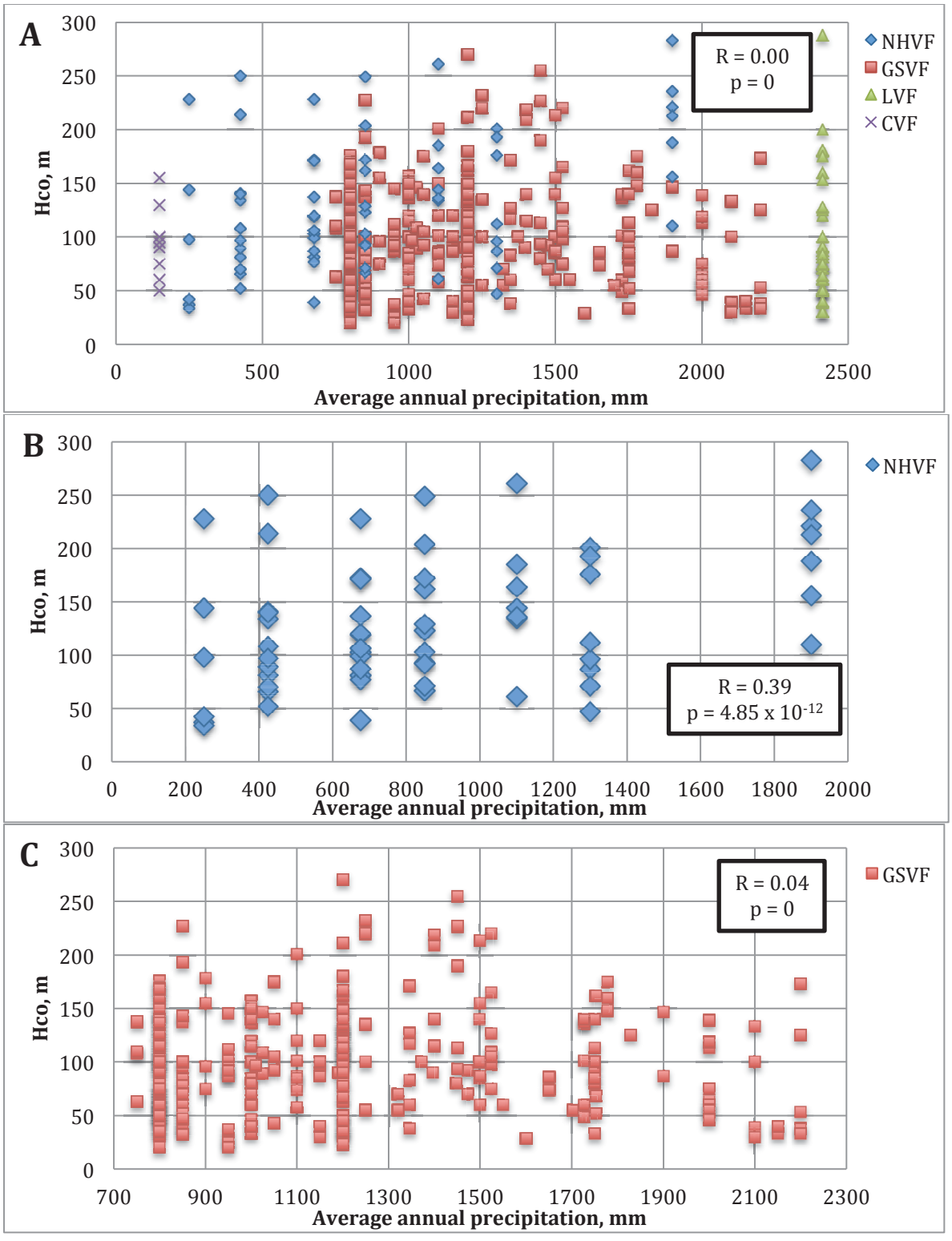

Figure 18: Summary of Hco in relation to the average annual precipitation. A) Hco of all study sites versus average annual precipitation. B) Hco of the NHVF versus average annual precipitation. C) Hco of GSVF versus average annual precipitation.

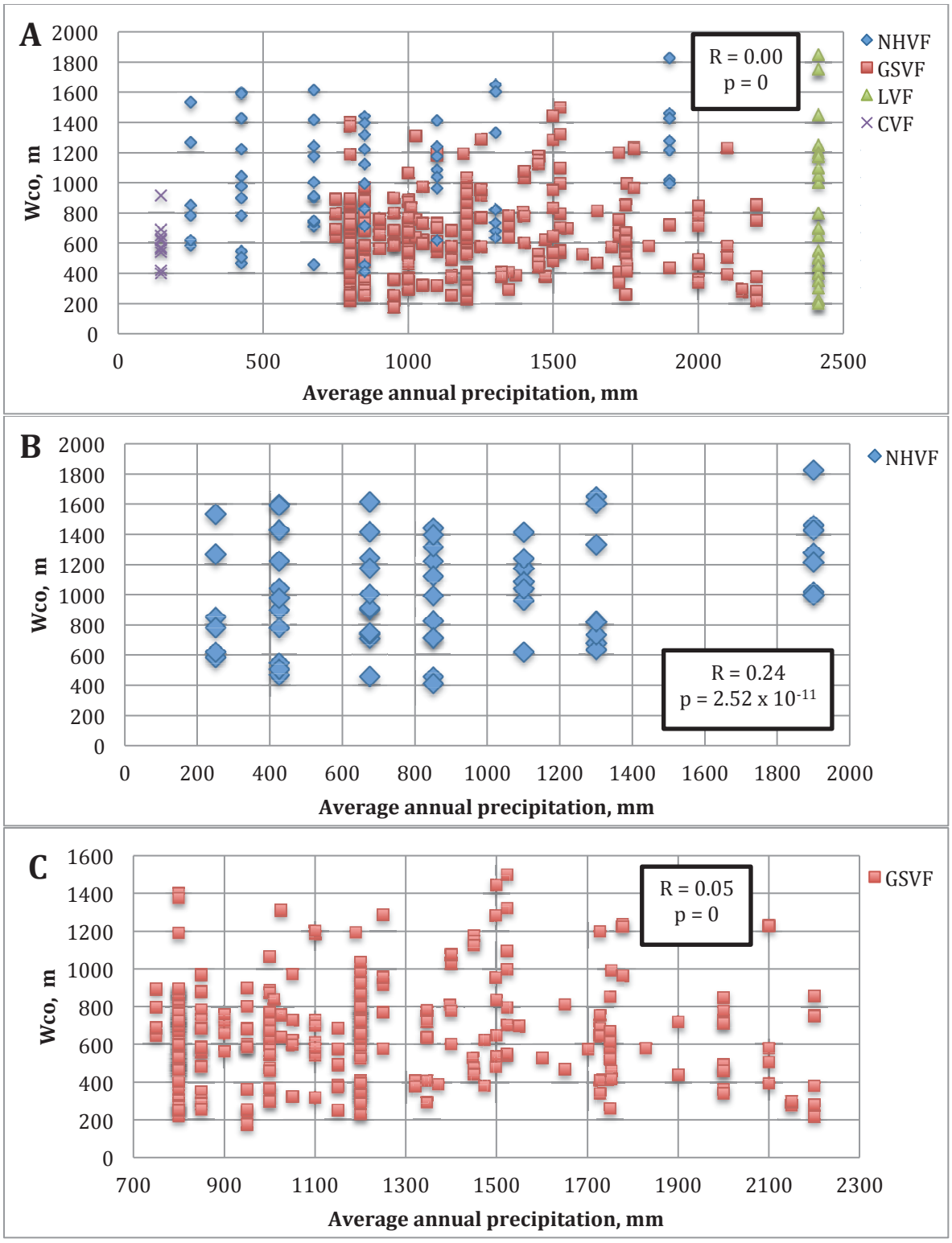

Figure 19: Summary of Wco in relation to the average annual precipitation. A) Wco of all study sites versus average annual precipitation. B) Hco of the NHVF versus average annual precipitation. C) Wco of GSVF versus average annual precipitation.

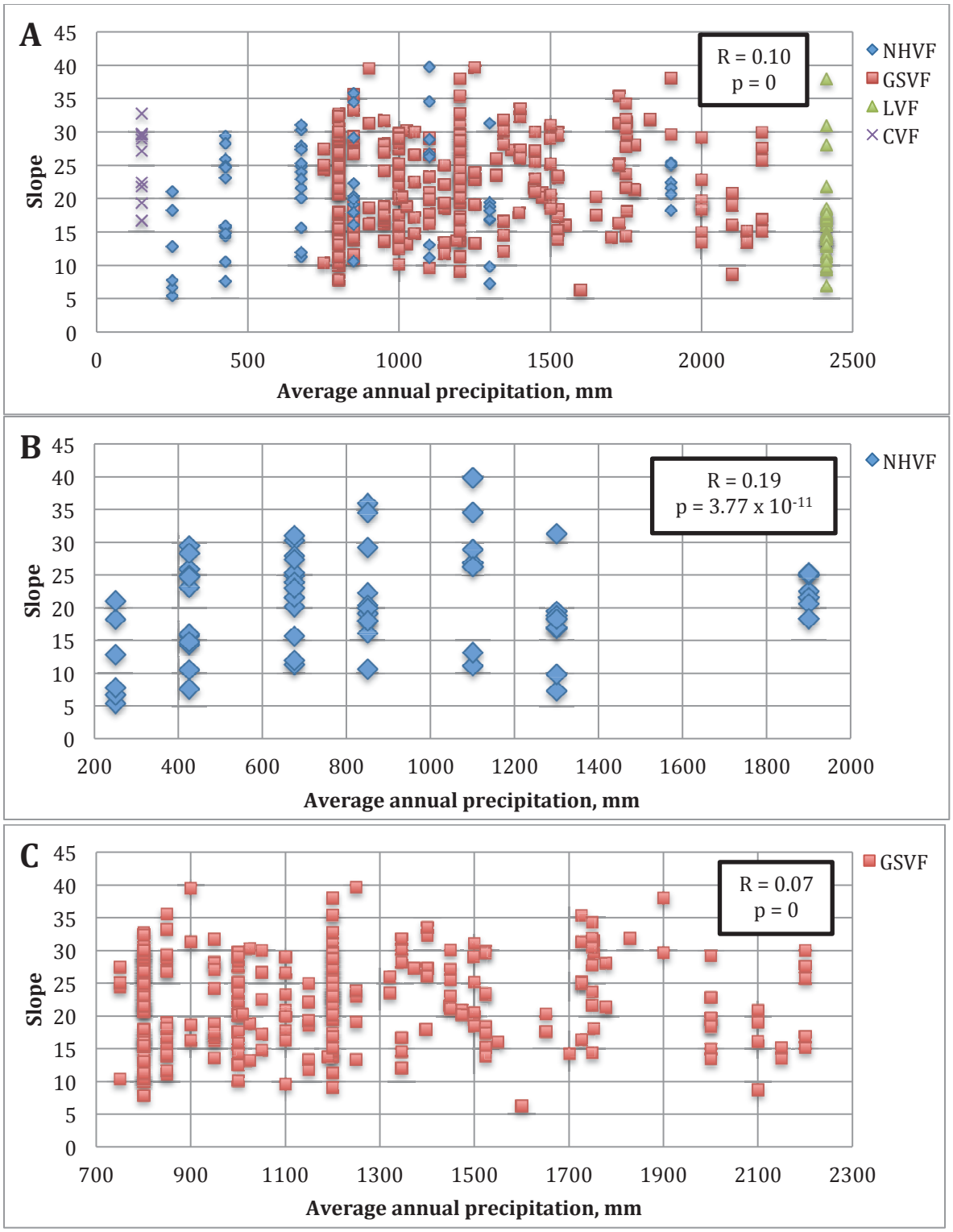

Figure 20: Summary of slope in relation to the average annual precipitation. A) Slope of all study sites versus average annual precipitation. B) Slope of the NHVF versus average annual precipitation. C) Slope of GSVF versus average annual precipitation.

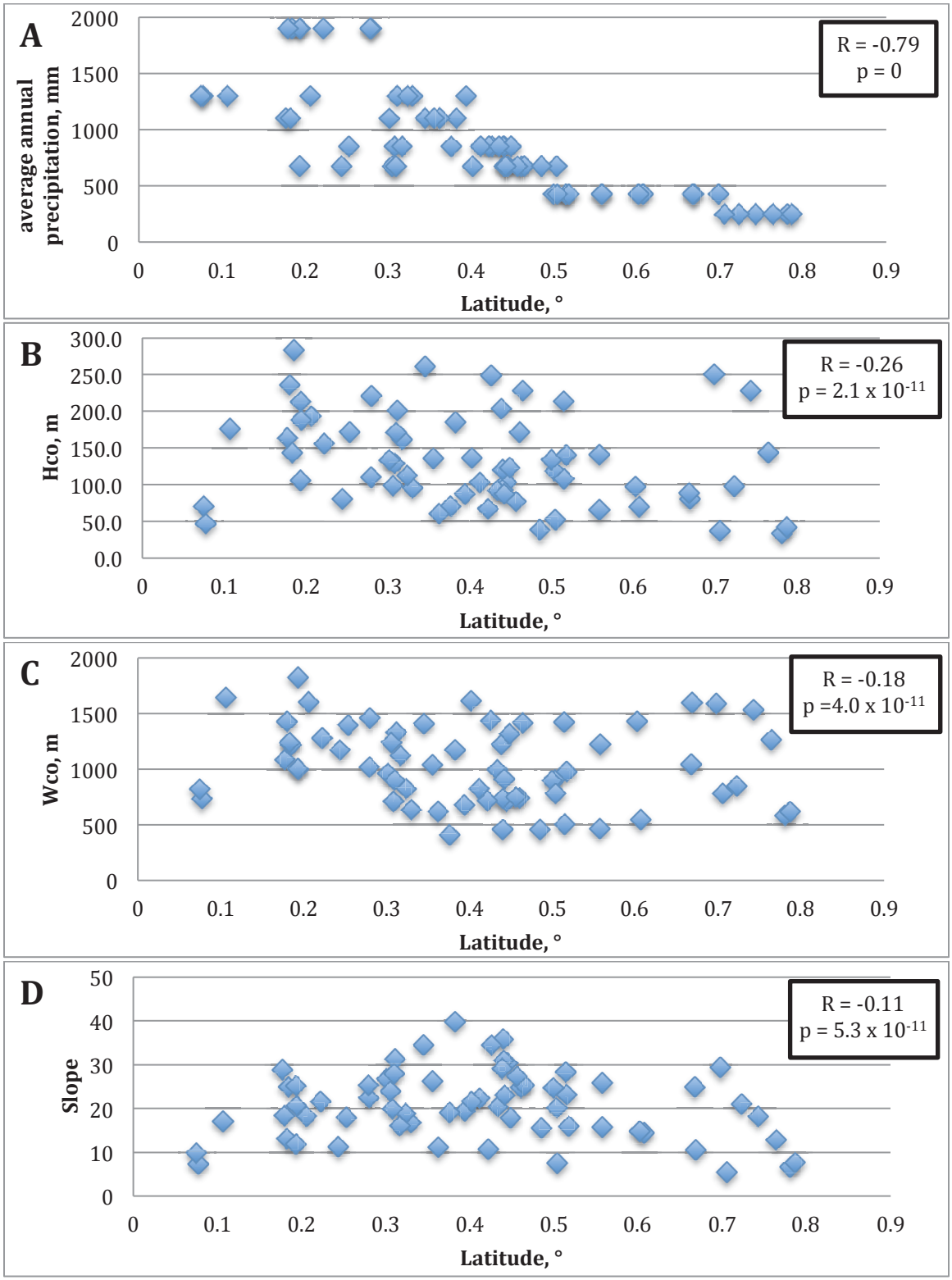

Figure 21: A) Average annual precipitation, B) Hco, C) Wco, and D) slope of the NHVF in relation to degrees of latitude

DISCUSSION

Cinder cone distribution and elongation

Within the NHVF there are numerous vent alignments (Brotzu et al., 1983; Hackman et al., 1990). Brotzu et al. (1983) observes that the majority of volcanic lineaments in the NHVF trend NNE-SSW, in addition to subordinate N-S, NW-SE, and E-W trends. All of these orientations are present in the Precambrian basement (Saggerson et al. 1960; Williams, 1966) and fieldwork by Rix (1967) documents NNE trending dikes projecting from the northern end of the NHVF. Elongated craters within the NHVF show the same NNE trend as volcanic lineaments. The coherence between volcanic lineaments and cone elongation is strong evidence that both reflect feeder dike geometry.

In the EARS complications arising from mechanical heterogeneity in the lithosphere, pre-existing structures, and 3-D interactions of magma with the lithosphere encumber researchers from distinguishing uniform system-wide kinematic trends. Morley (2010) distinguishes two end-member tectonic regimes from the literature: The regional extension model (Figure 22A) and the strike-slip model (Figure 22B). Analogue experiments, fault kinematic data, earthquake focal mechanisms, GPS, and fault characteristics generally support the regional extension model, with a maximum principle stress orientation of N13-15°E in map view (Corti et al., 2007; Delvaux and Barth, 2010; Keir et al., 2006; Stamps et al., 2008); however problems with the regional model remain including, most significantly, the pure-dip slip opening of NW-SE oriented grabens such as the Rukwa basin (Delvaux and Barth, 2010).

The NNE trend of dikes within the NHVF is only possible under the regional extension model. Under the strike slip model, feeder dikes would trend NE, causing elongated craters to form with a NE orientation as opposed to the NNE orientation observed in the NHVF. In map-view both dikes and earthquakes both form parallel to the maximum principle stress (Figure 1). In light of this, it is telling that the strikes of earthquake slip planes from an earthquake swarm in the Ethiopian section of the EARS that began October 2001 and ended January 2003 have a remarkably similar distribution and orientation to crater azimuths of elongation from the NHVF (Figure 23). This is strong evidence that cones in the NHVF formed under modern tectonic conditions.

Cones within the NHVF trend towards the higher types of the Corazzato and Tibaldi (2006) classification, based on both the low axial ratio of craters within the field and visual observations of cones in satellite imagery. Cones are expected to become more elongated when magma pressure is high or the compressive stress is very low (Corazzato and Tibaldi, 2006). High mama pressure enables dikes to form or re-open fractures oblique to the least compressive stress (Jolly and Sanderson, 1997; Le Corvec et al., 2013b; Rubin, 1995; Ziv et al., 2000) and although a variety of lineament orientations exist, the vast majority of aligned vents and elongated craters are oriented NNE-SSW, parallel to the least compressive stress predicted in the regional extension model. This suggests that the preponderance of cones in the NHVF towards higher, more elongated types is caused by the tectonic stress field rather than high magma pressure.

As summarized in the background, the wholesale distribution of an entire population of cinder cones reflects the shape of the magma source (Condit and Connor, 1996; Le Corvec et al., 2013b; Spörli and Eastwood, 1997). In the NHVF, there is a distinct change in cone distribution between the north and south ends of the field, best illustrated in the crater traces of Figure 15. In the north, cones are restricted to a narrow NE trending band that runs along the crest of the mini-dome. Cone density is lower in the south and vents are less clearly aligned, fanning out to the NW and SE. These differences might reflect variations in the shape of the magma source, or magma flux heterogeneity where the southern end of the field has high enough magma pressure to form dikes or re-open fractures at many orientations. Immediately to the southwest of the NHVF are volcanic lineaments stretching north from the polygenetic volcano Mount Kenya. Both Mount Kenya and the NHVF display the same uneven distribution of volcanism between the north and the south with the majority of volcanic deposits located in the south. In both fields the northern sector is characterized by the restriction of volcanism to a relatively narrow NE trending band composed primarily of volcanic lineaments. I believe the heterogeneous distribution of cinder cones between the north and the south reflects the centralization of magma over time first noted by Brotzu et al. 1983. According to geologic maps (Figure 24) the relatively youngest volcanic deposits are restricted to the south. It is possible that over time as the magmatic system evolved from fissure eruptions to centralized cinder cone forming eruptions magma pressures increased, as the magma supply was concentrated in the south. This would explain the higher

topography in the south, whether it resulted from an uneven volcanic pile or thermal elevation, and the diffuse distribution of cones in the south.

Morphological trends in the NHVF

The progressive change of slope, Hco/Wco, and volume moving away from the crest of the mini-dome is a relationship not documented elsewhere. The most likely explanation for this morphological pattern is that cones along the crest are the youngest and get older moving east or west. Although few radiometric ages are available for the NHVF (Brotzu et al., 1984; Opdyke et al., 2010), in geologic maps, the oldest volcanic units are only exposed at the fringes of the field (Figure 24). Moving towards the crest of the mini-dome reveals progressively younger volcanic deposits with the youngest flows restricted to a small area in the south. Although all the cones analyzed in this study are associated with the upper unit (2.1 my – recent), the geologic map is consistent with the hypothesis that the youngest cones are closest to the crest of the mini-dome. The considerable scatter in Hco/Wco at a given distance from the crest (Figure 14) may then reflect primary variation in cone shape.

The traditional age related decrease in Hco/Wco, documented by Wood (1980b) and Dohrenwend et al. (1986) results from a proportionately greater change in height than basal width. This is similar to the morphological pattern observed in the NHVF where a very small decrease in basal width is accompanied by a large decrease in height.

In an alternate hypothesis, if the morphological changes in the NHVF resulted from heterogeneous magma supply, where magma supply was plentiful at the crest and low at the edges of the field, the morphological trends would look very different to the ones observed. In this scenario, both cone height and basal width would decrease moving away from the center and slope would be unaffected. Cones in the NHVF, however, have a constant basal width, decreasing height, and decreasing slope with distance from the center consistent with the hypothesis that the youngest cones are located along the crest and age progressively moving east or west. Without radiometric ages it is impossible to confirm this hypothesis, however this age distribution is consistent with Brotzu et al., 1983 observation that the magmatic system has centralized over time.

Climatological controls on geomorphology

The GSVF and the NHVF provide a unique opportunity to study population wide effects of climate on cone geomorphology because both fields contain internal climate variability. In the GSVF there was no correlation between morphology and climate type. The NHVF did display some weak correlations between climate and morphology, most notably between average annual precipitation and height. Cinder cones in the NHVF are tallest in the wet, southern section of the field. This correlation remains when morphological changes in relation to the mini-dome are factored out (Figure 25).

However, in light of the mounting evidence supporting the centralization of the magmatic system including cinder cone distribution and morphology, the

presence of relatively tall cones in the south probably occurred not because of climate effects, but because of magma supply heterogeneity resulting from the centralization of the magmatic system in the south. According to geologic maps, southern cones are also the youngest and therefore likely to be the least eroded. This would also explain the presence of taller cones in the south.

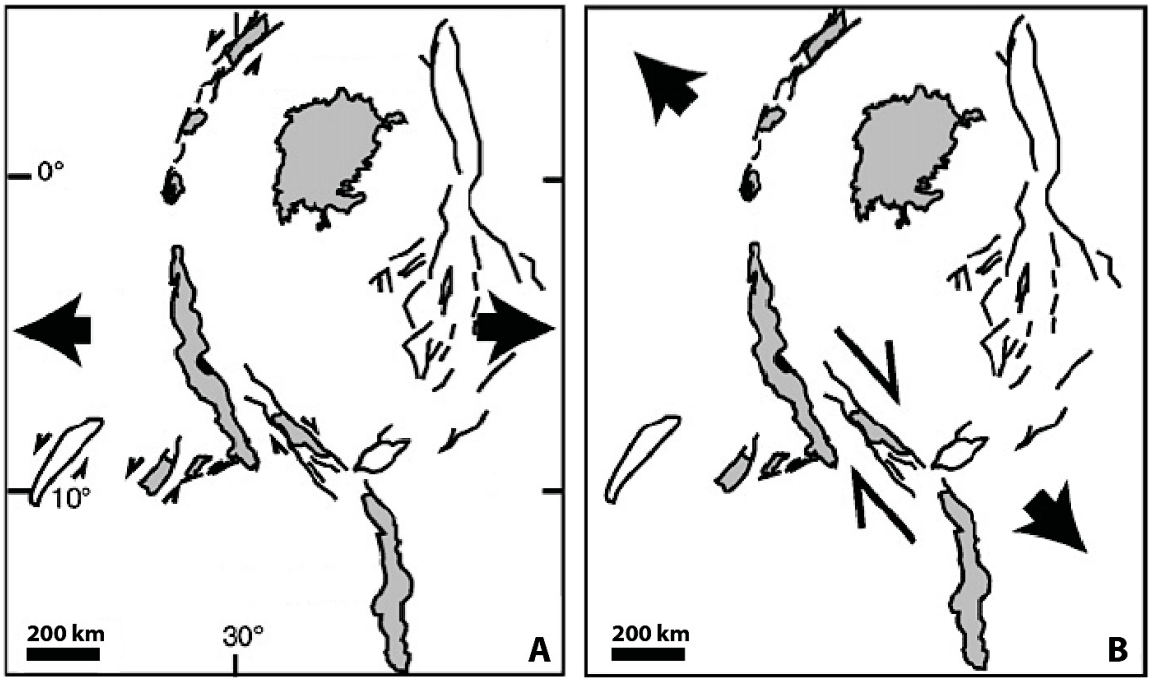

Figure 22: End member kinematic models of the EARS. A) Regional extension model showing E-W extension (e.g. Ebinger 1989; Morley, 1999) B) Strike-slip model showing NW-SE extension with significant dextral strike slip in southern segments (e.g. Chorowicz. 2005; Scott et al., 1989; Wheeler and Karson, 1994)

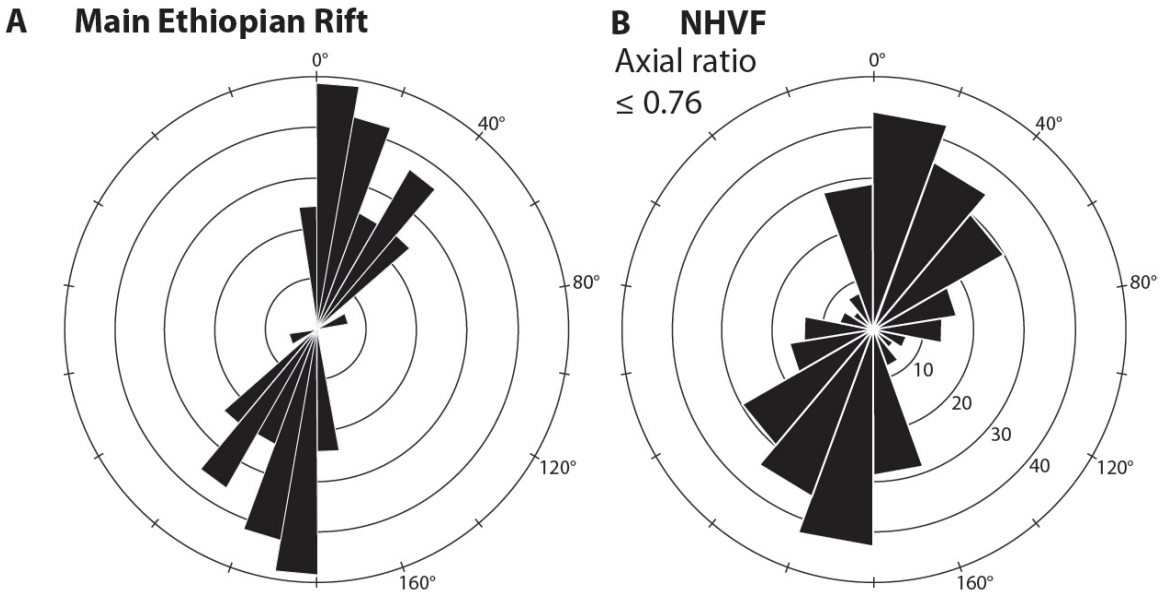

Figure 23: A) Strike of 1957 earthquake slip plane from swarm that began Oct 2001 and ended January 2003 in the Main Ethiopian Rift segment of the EARS. Modified from Keir et al., 2006. B) Azimuths of elongation of NHVF craters with an axial ratio ≤ 0.76.

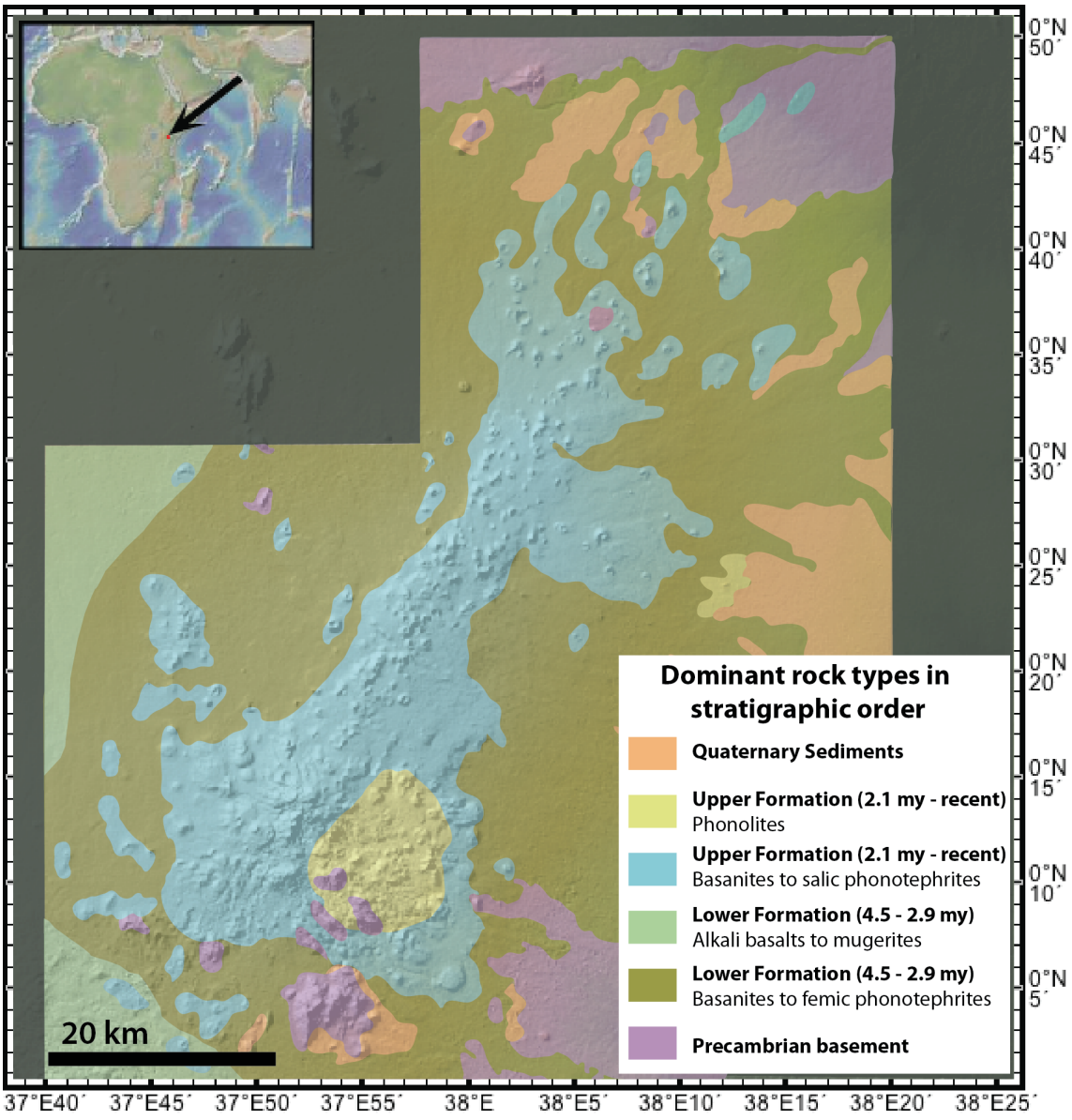

Figure 24: Geologic sketch map of the Nyambeni Hills Volcanic Field. Modified from Brotzu et al., 1983.

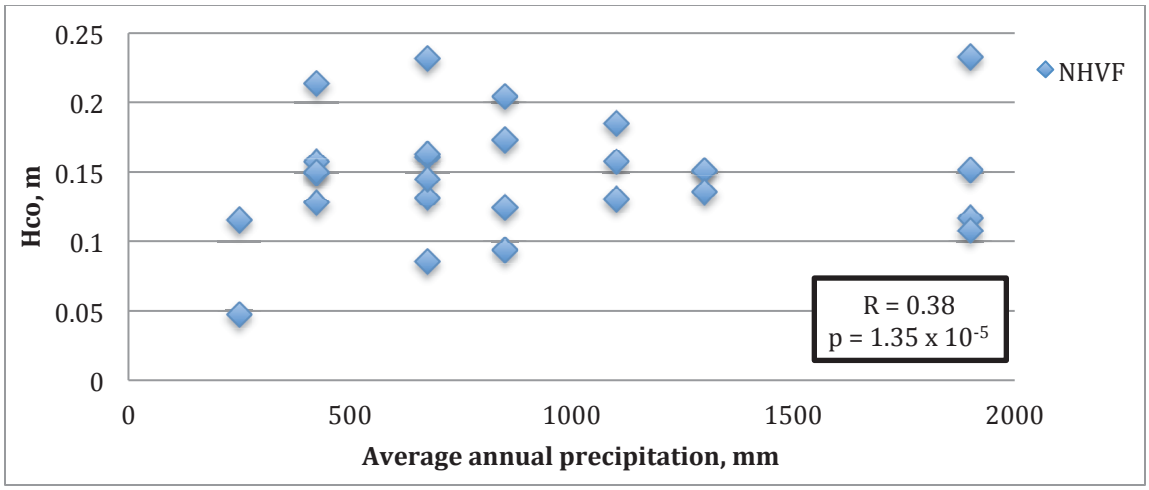

Figure 25: Hco of the NHVF versus average annual precipitation for cones < 5km from crest.

CONCLUSION

In the NHVF the geometry of the magmatic system and the tectonic regime are the strongest controls on cinder cone distribution and morphology. Volcanic lineament orientations and the direction of elongated cones are coherent with the regional extension model described by others (Delvaux and Barth, 2010; Keir et al., 2006; Stamps et al., 2008; Wolfenden et al., 2004). This tectonic regime must have been persistent over the duration of cinder cone formation from approximately 2.1 Ma until recent times.

Morphological trends in relation to the mini-dome crest are probably caused by younging at the center of the field. This, along with differences in cinder cone distribution between the north and south support the hypothesis of Brotzu et al. (1983) that magmatic activity centralized over time and is now concentrated in the south. Radiometric studies are required to confirm this hypothesis and future work might consider investigating the relationship between cone elongation and age to see if it is possible to observe morphological changes in relation to the shift from fissure eruptions to cinder cone eruptions.

The off-axis volcanic fields of the Kenyan segment of the EARS share many traits with the NHVF. These include characteristics such as: the restriction of cones to a narrow NE trending band, the presence of a NE trending mini-dome, a two phase eruptive history beginning in the late Miocene with a fissure dominant shield building phase, followed by a mid-Pliocene cinder cone phase (Brotzu et al., 1984), and in the case of the Hurri Hills, Marsabit and the Chyulu hills, being centered at 38° longitude. The similarities in spatial trends, timing, and longitude hint at a

unifying underlying mechanism whose relationship to axial rifting is unknown. Implications from this study about the magmatic system in the NHVF could be applied to other off-axis fields.

Over millions of years the effects of weathering on cone morphology is the same between wet and dry areas. This might not be the case over the short term but radiometric ages and higher resolution data are needed to be sure. In general, the comparison of the four volcanic fields of this study supported the importance of tectonic setting in controlling cone morphology consistent with the conclusions of Fornaciai et al. (2012), Tibaldi (1995), and Corazzato and Tibaldi (2006). The one possible exception, the LVF, hails from the wettest and warmest climate zone, suggesting that, in some cases, climate might impact morphological trends, namely erosion rate.

REFERENCES

Anderson, E. M., 1951, The Dynamics of Faulting and Dyke Formation with Applications to Britain, Oliver and Boyd, London, U.K.

Aurisicchio, C., Brotzu, P., Morbidelli, L., Piccirillo, E.M., Traversa, G., 1983. Basanite to peralkaline phonolite suite: Quantitative crystal fractionation model (Nyambeni range, East Kenya Plateau). Neues Jahrbuch fur Mineralogie - Abhandlungen 148, 113–140.

Bartley, J.M., Glazner, A.F., Schermer, E.R., 1990. North-South Contractions of the Mojave Block and Strike-Slip Tectonics in Southern California. Science 248, 1398–1401.

Bemis, K., Walker, J., Borgia, A., Turrin, B., Neri, M., Swisher, C., III, 2011. The growth and erosion of cinder cones in Guatemala and El Salvador: Models and statistics. Journal of Volcanology and Geothermal Research 201, 39–52. doi:10.1016/j.jvolgeores.2010.11.007

Bosworth, W., 1987. Off-axis volcanism in the Gregory rift, east Africa: implications for models of continental rifting. Geology.

Brotzu, P., Cagliari, L.M., Rome, E.M., 1983. The basanite to peralkaline phonolite suite of the plioquaternary Nyambeni multicentre volcanic range (East Kenya Plateau). Neues Jahrbuch fur Mineralogie - Abhandlungen 147, 253–280.

Brotzu, P., Morbidelli, L., Nicoletti, M., Piccirillo, E., Traversa, G., 1984. Miocene to Quaternary volcanism in eastern Kenya: sequence and geochronology. Tectonophysics 101, 75–86.

Burkart, B., Self, S., 1985. Extension and rotation of crustal blocks in northern Central America and effect on the volcanic arc. Geology 13, 22–26.

Carn, S.A., 1999. Application of synthetic aperture radar (SAR) imagery to volcano mapping in the humid tropics: a case study in East Java, Indonesia. Bull Volcanol 61, 92–105.

Carn, S.A., 2000. The Lamongan volcanic field, East Java, Indonesia: physical volcanology, historic activity and hazards. Journal of Volcanology and Geothermal Research 95, 81–108.

Carr, M.J., Feigenson, M.D., Patino, L.C., Walker, J.A., 2003. Volcanism and geochemistry in Central America: Progress and problems. Geophysical Monograph 138 153–174. doi:10.1029/138GM09

Chorowicz, J., 2005. The East African rift system. Journal of African Earth Sciences 43, 379–410. doi:10.1016/j.jafrearsci.2005.07.019

Condit, C.D., Connor, C.B., 1996. Recurrence rates of volcanism in basaltic volcanic fields: An example from the Springerville volcanic field, Arizona. Geological Society of America Bulletin 108, 1225–1241.

Corazzato, C., Tibaldi, A., 2006. Fracture control on type, morphology and distribution of parasitic volcanic cones: An example from Mt. Etna, Italy. Journal of Volcanology and Geothermal Research 158, 177–194. doi:10.1016/j.jvolgeores.2006.04.018

Corti, G., van Wijk, J., Cloetingh, S., Morley, C.K., 2007. Tectonic inheritance and continental rift architecture: Numerical and analogue models of the East African Rift system. Tectonics 26, 1–13. doi:10.1029/2006TC002086

Delaney, P.T., Pollard, D.D., Ziony, J.I., McKee, E.H., 1986. Field relations between dikes and joints: Emplacement processes and paleostress analysis. Journal of Geophysical Research 91, 4920–4938.

Delvaux, D., Barth, A., 2010. African stress pattern from formal inversion of focal mechanism data. Tectonophysics 482, 105–128. doi:10.1016/j.tecto.2009.05.009

Dohrenwend, J.C., McFadden, L.D., Turrin, B.D., Stephen, W.G., 1984. K-Ar dating of the Cima volcanic field, eastern Mojave Desert, California: Late Cenozoic volcanic history and landscape evolution. Geology 12, 163–167.

Dohrenwend, J.C., Wells, S.G., Turrin, B.D., 1986. Degradation of Quaternary cinder cones in the Cima volcanic field, Mojave Desert, California. Geological Society of America Bulletin 97, 421–427.

Ebinger, C.J., 1989. Tectonic development of the western branch of the East African rift system. Geological Society of America Bulletin 101, 885–903.

Favalli, Massimilano, Karátson, D., Mazzarini, F., Pareschi, M.T., Boschi, E., 2009. Morphometry of scoria cones located on a volcano flank: A case study from Mt. Etna (Italy), based on high-resolution LiDAR data. Journal of Volcanology and Geothermal Research 186, 320–330. doi:10.1016/j.jvolgeores.2009.07.011

Favalli, Massimiliano, Pareschi, M.T., 2004. Digital elevation model construction from structured topographic data: The DEST algorithm. Journal of Geophysical Research 109, 1–17. doi:10.1029/2004JF000150

Fornaciai, A., Favalli, M., Karátson, D., Tarquini, S., Boschi, E., 2012. Morphometry of scoria cones, and their relation to geodynamic setting: A DEM-based analysis. Journal of Volcanology and Geothermal Research 217-218, 56–72. doi:10.1016/j.jvolgeores.2011.12.012

Guzmán-Speziale, M., 2001. Active seismic deformation in the grabens of northern Central America and its relationship to the relative motion of the North America–Caribbean plate boundary. Tectonophysics 337, 39–51.

Hackman, B.D., Charsley, T.J., Key, R.M., Wilkinson, A.F., 1990. The development of the East African Rift system in north-central Kenya. Tectonophysics 184, 189–211.

Hasenaka, T., Carmichael, I.S.E., 1985a. The cinder cones of Michoacán—Guanajuato, central Mexico: their age, volume and distribution, and magma discharge rate. Journal of Volcanology and Geothermal Research 25, 105–124.

Hasenaka, T., Carmichael, I.S.E., 1985b. A compilation of location, size, and geomorphological parameters of volcanoes of the Michoacan-Guanajuato volcanic field, central Mexico. Geofísica Internacional 24-4, 577–607.

Hooper, D.M., Sheridan, M.F., 1998. Computer-simulation models of scoria cone degradation. Journal of Volcanology and Geothermal Research 83, 241–267.

Inbar, M., Risso, C., 2001. A morphological and morphometric analysis of a high density cinder cone volcanic field-Payun Matru, south-central Andes, Argentina. Zeitschrift fuer Geomorphologie - Annals of Geomorphology 45, 321–343.

Jolly, R., Sanderson, D.J., 1997. A Mohr circle construction for the opening of a pre-existing fracture. Journal of Structural Geology 19, 887–892.

Kamau, J.N., Kinyua, R., Gathua, J.K., 2010. 6 years of wind data for Marsabit, Kenya average over 14m/s at 100m hub height; An analysis of the wind energy

potential. Renewable Energy 35, 1298–1302. doi:10.1016/j.renene.2009.10.008
Keir, D., Ebinger, C.J., Stuart, G.W., Daly, E., Ayele, A., 2006. Strain accommodation by magmatism and faulting as rifting proceeds to breakup: Seismicity of the northern Ethiopian rift. Journal of Geophysical Research 111, 1–17. doi:10.1029/2005JB003748
Kereszturi, G., Geyer, A., Martí, J., Németh, K., Dóniz-Páez, F.J., 2013. Evaluation of morphometry-based dating of monogenetic volcanoes—a case study from Bandas del Sur, Tenerife (Canary Islands). Bull Volcanol 75, 734. doi:10.1007/s00445-013-0734-1
Kereszturi, G., Németh, K., 2012. Monogenetic Basaltic Volcanoes: Genetic Classification, Growth, Geomorphology and Degradation, in: Updates in Volcanology - New Advances in Understanding Volcanic Systems. InTech, pp. 3–89. doi:10.5772/51387
Kervyn, M., Ernst, G.G.J., Carracedo, J.C., Jacobs, P., 2012. Geomorphometric variability of "monogenetic" volcanic cones: Evidence from Mauna Kea, Lanzarote and experimental cones. Geomorphology 136, 59–75. doi:10.1016/j.geomorph.2011.04.009
Le Corvec, N., Menand, T., Lindsay, J., 2013a. Interaction of ascending magma with pre-existing crustal fractures in monogenetic basaltic volcanism: an experimental approach. J. Geophys. Res. Solid Earth 118, 1–17. doi:10.1002/jgrb.50142
Le Corvec, N., Spörli, K.B., Rowland, J., Lindsay, J., 2013b. Spatial distribution and alignments of volcanic centers: Clues to the formation of monogenetic volcanic fields. Earth Science Reviews 124, 96–114. doi:10.1016/j.earscirev.2013.05.005
Lyon-Caen, H., Barrier, E., Lasserre, C., Franco, A., Arzu, I., Chiquin, L., Chiquin, M., Duquesnoy, T., Flores, O., Galicia, O., Luna, J., Molina, E., Porras, O., Requena, J., Robles, V., Romero, J., Wolf, R., 2006. Kinematics of the North American–Caribbean-Cocos plates in Central America from new GPS measurements across the Polochic-Motagua fault system. Geophys. Res. Lett. 33, L19309. doi:10.1029/2006GL027694
Maguire, P., Swain, C.J., Masotti, R., Khan, M.A., 1994. A crustal and uppermost mantle cross-sectional model of the Kenya Rift derived from seismic and gravity data. Tectonophysics 236, 217–249.
Martin, U., Németh, K., 2006. How Strombolian is a "Strombolian" scoria cone? Some irregularities in scoria cone architecture from the Transmexican Volcanic Belt, near Volcán Ceboruco, (Mexico) and Al Haruj (Libya). Journal of Volcanology and Geothermal Research 155, 104–118. doi:10.1016/j.jvolgeores.2006.02.012
Mazzarini, F., 2004. Volcanic vent self-similar clustering and crustal thickness in the northern Main Ethiopian Rift. Geophys. Res. Lett. 31, 1–4. doi:10.1029/2003GL018574
McGetchin, T.R., Settle, M., Chouet, B.A., 1974. Cinder cone growth modeled after northeast crater, Mount Etna, Sicily. Journal of Geophysical Research 79, 3257–3272.
Meyer, D.J., Tachikawa, T., Abrams, M., Crippen, R., Krieger, T., Gesch, D., Carabajal, C., 2012. Summary of the validation of the second version of the ASTER GDEM. International Archives of the Photogrammetry, Remote Sensing, and Spatial

Information Sciences.
Morley, C.K., 1999. AAPG Studies in Geology# 44, Chapter 9: Influence of Preexisting Fabrics on Rift Structure. AAPG studies in geology 44, 151–160.
Morley, C.K., 2010. Stress re-orientation along zones of weak fabrics in rifts: An explanation for pure extension in "oblique" rift segments? Earth and Planetary Science Letters 297, 667–673. doi:10.1016/j.epsl.2010.07.022
Opdyke, N.D., Kent, D.V., Huang, K., Foster, D.A., Patel, J.P., 2010. Equatorial paleomagnetic time-averaged field results from 0–5 Ma lavas from Kenya and the latitudinal variation of angular dispersion. Geochem. Geophys. Geosyst. 11, 1–20. doi:10.1029/2009GC002863
Paulsen, T.S., Wilson, T.J., 2010. New criteria for systematic mapping and reliability assessment of monogenetic volcanic vent alignments and elongate volcanic vents for crustal stress analyses. Tectonophysics 482, 16–28. doi:10.1016/j.tecto.2009.08.025
Porter, S.C., 1972. Distribution, morphology, and size frequency of cinder cones on Mauna Kea Volcano, Hawaii. Geological Society of America Bulletin 83, 3607–3612.
Puspito, N.T., Shimazaki, K., 1995. Mantle structure and seismotectonics of the Sunda and Banda arcs. Tectonophysic 251, 215–228.
Rech, J.A., Reeves, R.W., Hendricks, D.M., 2001. The influence of slope aspect on soil weathering processes in the Springerville volcanic field, Arizona. Catena 43, 49–62.
Riedel, C., Ernst, G.G.J., Riley, M., 2003. Controls on the growth and geometry of pyroclastic constructs. Journal of Volcanology and Geothermal Research 127, 121–152. doi:10.1016/S0377-0273(03)00196-3
Rix, P., 1967. Geology of the Kinna area (No. 81). Geological Survey of Kenya.
Rubin, A.M., 1995. Propagation of magma-filled cracks. Annual Review of Earth and Planetary Sciences 23, 287–336.
Scott, D.L., Rosendahl, B.R., Burgess, C.F., Sander, S., 1989. Comments on "Variable extension in Lake Tanganyika" by CK Morley. Tectonics 8, 647–650.
Settle, M., 1979. The structure and emplacement of cinder cone fields. American Journal of Science 279, 1089–1107.
Sombroek, W.G., Braun, H.M.H., Van der Pouw, B.J.A., 1982. Exploratory Soil Map and Agro-climatic Zone Map of Kenya, 1980.
Spörli, K.B., Eastwood, V.R., 1997. Elliptical boundary of an intraplate volcanic field, Auckland, New Zealand. Journal of Volcanology and Geothermal Research 79, 169–179.
Stamps, D.S., Calais, E., Saria, E., Hartnady, C., Nocquet, J.-M., Ebinger, C.J., Fernandes, R.M., 2008. A kinematic model for the East African Rift. Geophys. Res. Lett. 35, 1–6. doi:10.1029/2007GL032781
Tibaldi, A., 1995. Morphology of pyroclastic cones and tectonics. Journal of Geophysical Research 100, 24521–24535.
Valentine, G.A., Gregg, T.K.P., 2008. Continental basaltic volcanoes — Processes and problems. Journal of Volcanology and Geothermal Research 177, 860–876. doi:10.1016/j.jvolgeores.2008.01.050
Walker, J.A., Singer, B.S., Jicha, B.R., Cameron, B.I., Carr, M.J., Olney, J.L., 2011.

Monogenetic, behind-the-front volcanism in southeastern Guatemala and western El Salvador: 40Ar/39Ar ages and tectonic implications. LITHOS 123, 243–253. doi:10.1016/j.lithos.2010.09.016

Wheeler, W.H., Karson, J.A., 1994. Extension and subsidence adjacent to a“ weak” continental transform: An example from the Rukwa rift, East Africa. Geology 22, 625–628.

Williams, L.A.J., 1966. Geology of the Chanler's Falls area (No. 75). Geological Survey of Kenya.

Wolfenden, E., Ebinger, C., Yirgu, G., Deino, A., Ayalew, D., 2004. Evolution of the northern Main Ethiopian rift: birth of a triple junction. Earth and Planetary Science Letters 224, 213–228. doi:10.1016/j.epsl.2004.04.022

Wood, C.A., 1980a. Morphometric evolution of cinder cones. Journal of Volcanology and Geothermal Research 7, 387–413.

Wood, C.A., 1980b. Morphometric analysis of cinder cone degradation. Journal of Volcanology and Geothermal Research 8, 137–160.

Ziv, A., Rubin, A.M., Agnon, A., 2000. Stability of dike intrusion along preexisting fractures. Journal of Geophysical Research 105, 5947–5961.

Appendix 1: World map of Köppen-Geiger climate classification

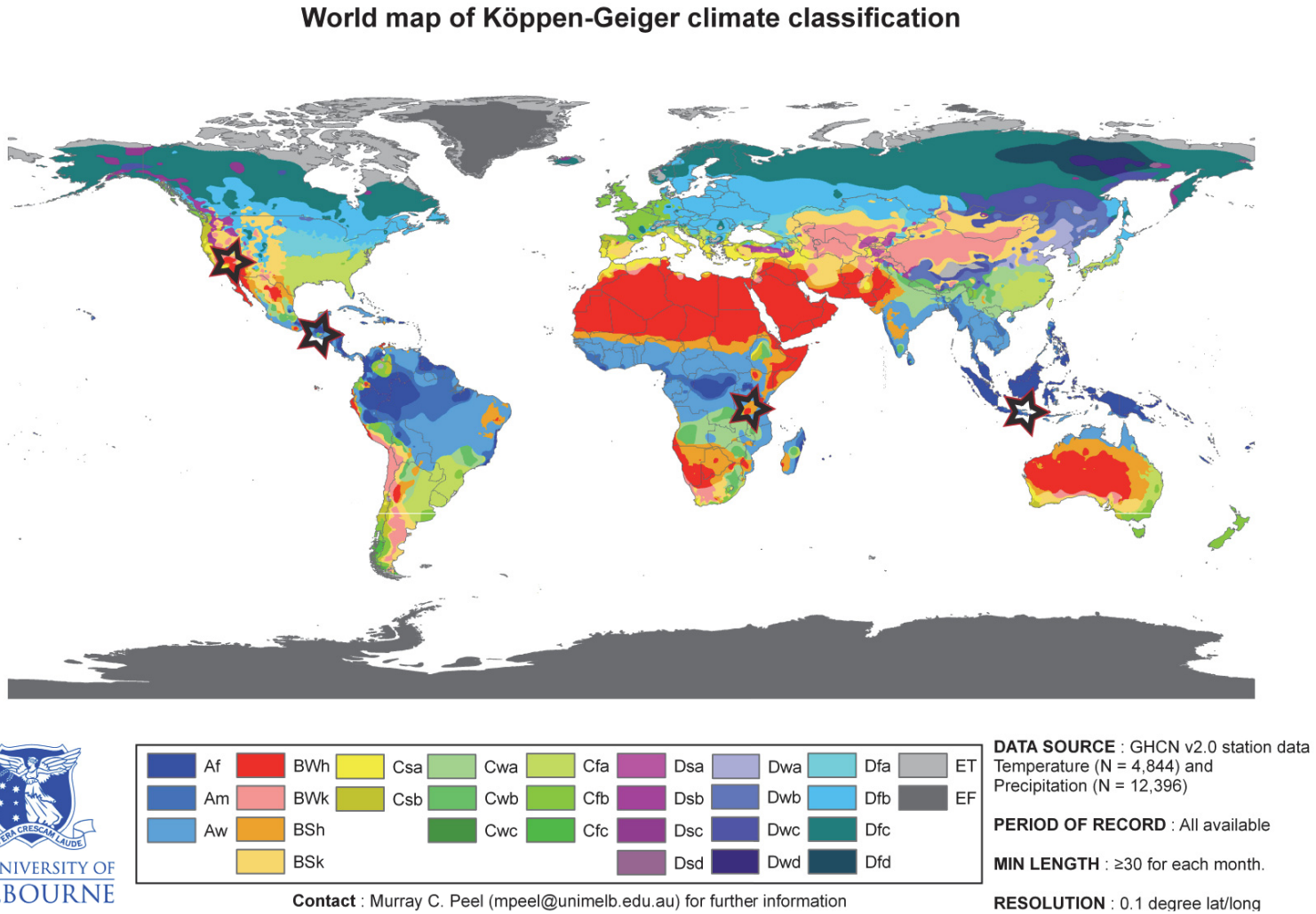

Appendix 2: Agro-climatic zone map of Kenya

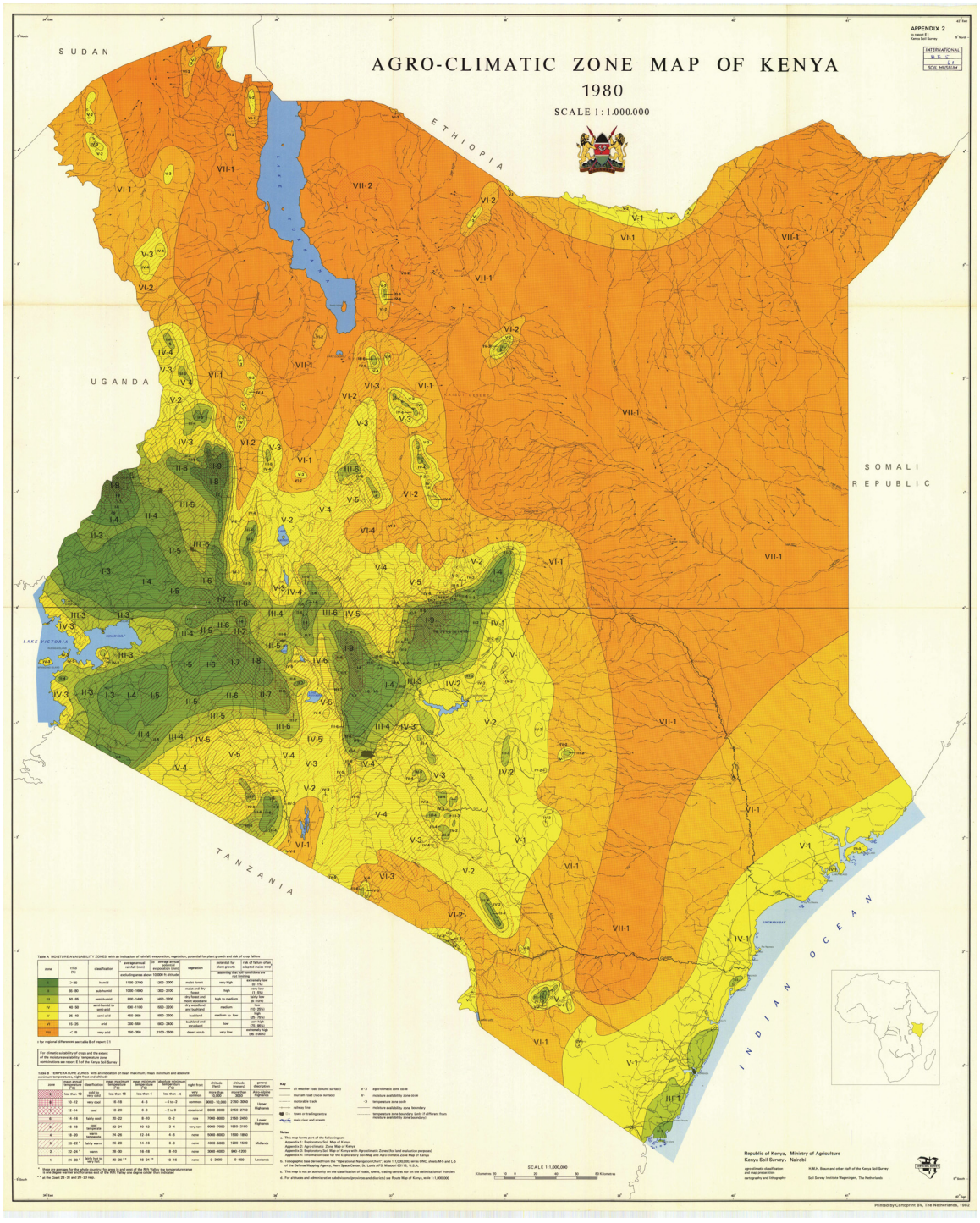

Appendix 3: Average annual precipitation map of Guatemala